This is to certify that the

thesis entitled

ESEEM Studies of the Oxygen Evolving Complex of Photosystem II

presented by

Michelle Mac

has been accepted towards fulfillment of the requirements for

M.S. degree in Chemistry

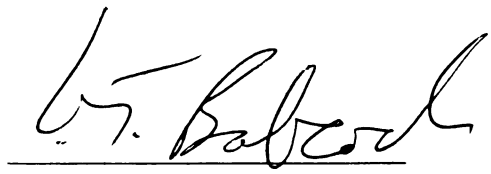

Major professor

Date Nov 10, 1992

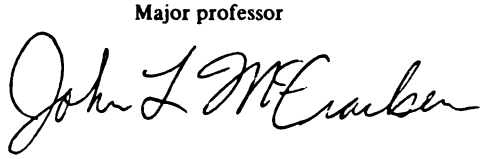

ESEEM STUDIES OF THE OXYGEN EVOLVING COMPLEX OF PHOTOSYSTEM II

By

Michelle Mac

A THESIS

Submitted to
Michigan State University
in partial fulfillment of the requirements
for the degree of

MASTER OF SCIENCE

Department of Chemistry

1993

ABSTRACT

ESEEM STUDIES OF THE OXYGEN EVOLVING COMPLEX OF PHOTOSYSTEM II

By

Michelle Mac

Photosystem II (PS II) is the enzyme in photosynthesis which catalyzes the oxidation of water. Water oxidation chemistry is thought to be performed by a membrane bound oxygen evolving complex (OEC) containing manganese. The use of a refined biochemical preparation which increases the concentration of PS II present in a sample has facilitated study of the Mn multiline EPR spectrum associated with the OEC. This spectrum has been studied by using magnetic resonance techniques. EPR studies discussed in this thesis have shown that the reaction center complex (RCC) samples are spectroscopically equivalent to their predessors. The increased concentration achieved with the RCCs is essential for EPR analysis. Slight modifications of the published RCC procedure were made as a result of this increased concentration. It has been shown previously that substitution of Sr^{2+} or chelator into calcium depleted BBY samples causes modifications in the hyperfine splitting seen in the multiline spectrum. These differences are thought to arise from perturbations of the Mn exchange coupling. These differences were present in the multiline spectra from the RCC samples presented in this thesis. ESEEM studies of the RCC samples were also performed. A 4 MHz peak, thought to arise from coupling to a ligated nitrogen, is present in all spectra recorded. This indicates a conformational change that does not affect the interactions of the Mn with its environment. Additional magnetic resonance studies will be performed to determine the magnitude of these interactions.

ACKNOWLEDGEMENTS

I would like to thank both Dr. Jerry Babcock and Dr. John McCracken for their guidance in this project.

I would also like to thank all the members of the Babcock and McCracken research groups, and in particular, Kerry Reidy for her encouragement and "impromptu" quantum mechanics discussions.

I would especially like to thank Matt Espe for his time, patience and friendship. His teaching and knowledge were invaluable to me and this thesis could not have been completed without him.

Lastly, I would like to thank my parents for their love and encouragement.

M.M.

TABLE OF CONTENTS

LIST OF FIGURES

Chapter 1
Introduction

Although photosynthesis has been studied extensively since the discovery of oxygen evolution from plants in 1780 by Joseph Priestley, many of the molecular intricacies of the process remain an enigma. The mechanism of photosynthesis utilizes photochemical energy from sunlight to disrupt chemical bonds in stable substrates. The free energy inherent in this process can be trapped by the organism to synthesize vital amino acids, proteins and other biomolecules. Molecular oxygen is released by higher plants as a by-product of the reaction. The process can be described with a deceptively simple reaction:

$$CO_2 + H_2O \text{ ----------> } (CH_2O)_n + O_2$$

The mechanism behind this reaction however, is complex and requires the interplay of many proteins and cofactors, many of which have not been completely characterized.

There are two types of pigment-protein complexes, called reaction centers, that convert light energy into chemically useful energy in higher plants. The first of these, Photosystem I (PSI) mediates the production of oxidized plastocyanin and reduced NADP. This NADPH produced is used to fuel the enzymatic cycles associated with the assimilation of carbon dioxide in the Calvin cycle. The second reaction center, the Photosystem II/oxygen evolving complex (PS II/OEC), is associated with water oxidation and the evolution of oxygen. Both of these systems are represented schematically in Figure 1. This model, known as the Z-scheme, represents the flow of electron transport in plants and cyanobacteria.[1] The vertical position of each electron carrier corresponds to its reduction potential at pH=7.0.

An interesting aspect of the electron transfer process in photosynthesis is its vectorial nature. The photosynthetic machinery is located, in higher plants, in an organelle known as the chloroplast. Chloroplasts are similar in structure to the

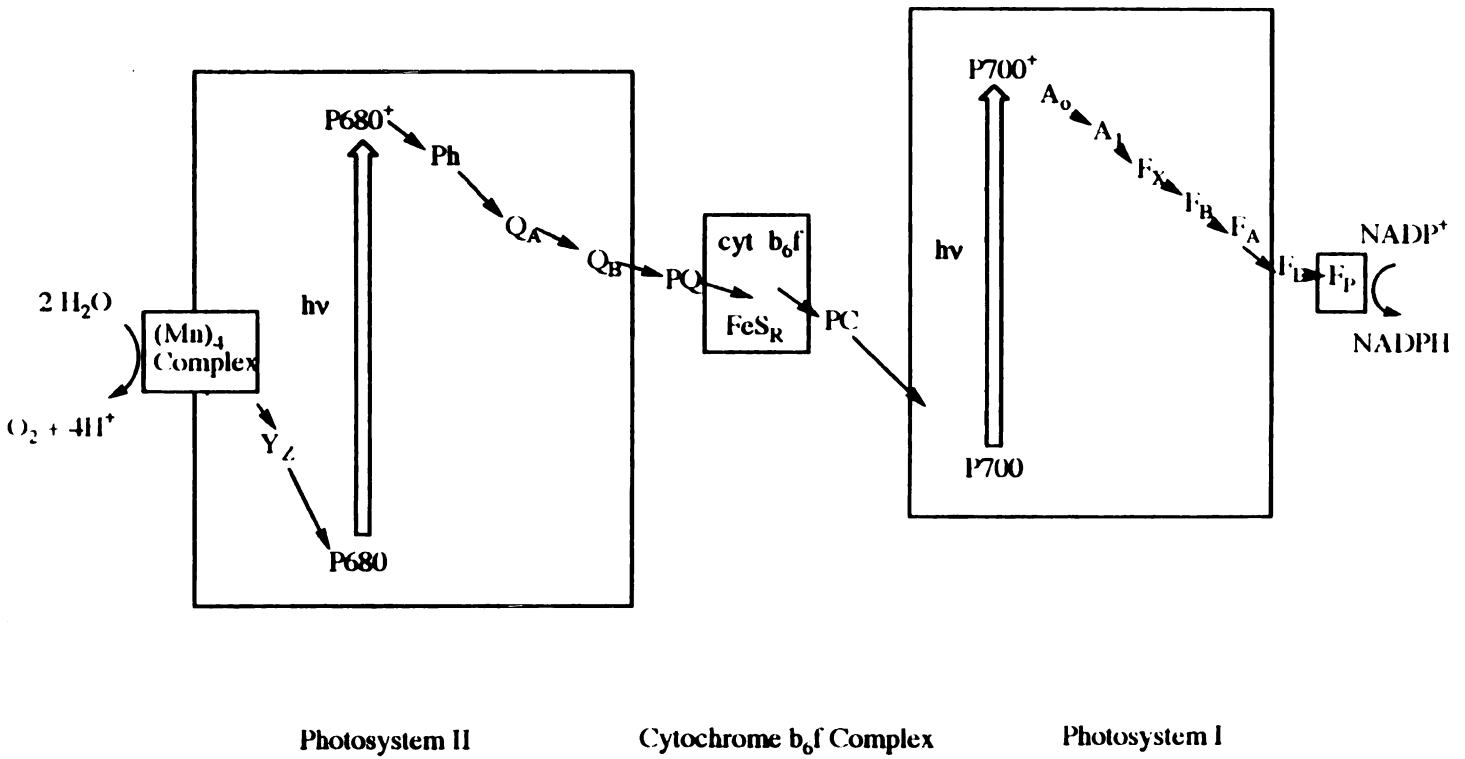

Figure 1: The Z scheme of photosynthesis representing non-cyclic electron flow in higher plants.

mitochondria of animals in that they contain both an inner and outer membrane. The inner membrane surrounds an aqueous protein matrix which contains membranous structures called thylakoid membranes. These closed vesicles separate two chemically different environments: the stroma, located on the exterior of the thylakoid membranes and the lumen, located on the interior. These appear on electron micrographs as flattened sack-like structures and are "stacked" in certain regions of the chloroplast.[2] It has been shown that as much as 85% of the PS II reaction centers are concentrated in these stacked regions, called grana.[2] Photosystem I is not, however, in the same location in the thylakoids as PS II. It is found, instead, in the unstacked stromal regions of the thylakoid. This asymmetric arrangement assists in providing directionality to the electron flow. It also results in both charge and proton gradients across the photosynthetic membrane that ultimately provide the free energy necessary for ATP synthesis.

As seen in Figure 1, PS I and PS II are linked through electron transfer reactions. However, due to their different locations in the thylakoid membrane, an additional membrane bound complex is required to mediate their interaction. Cytochrome b_6f (cyt b_6f) is distributed evenly in the chloroplast between the grana (PS II) and the unstacked regions (PS I) and therefore seems like an ideal charge transfer interface between PS II and PS I. The cytochrome is too large to readily diffuse the distances needed for transportation of electron equivalents between PS II and PS I, especially on the timescale of intersystem electron transfer. The lateral communication between reaction centers is performed by a small (MW=10.5 kDa) copper protein called plastocyanin.

Structure

A better understanding of the functional aspects of the PS II/OEC can be obtained with an in depth discussion of the polypeptides and co-factors associated with this membrane bound complex. There are less than twenty polypeptides associated with the

PS II/OEC, making it a moderately complex system.[3] This complexity, however, is remarkably easy to resolve biochemically. Detergent solubilization methods have allowed isolation of a number of smaller assemblies which have lead to the construction of a reasonable working model of the PS II/OEC. This postulated model which shows relevant polypeptides and co-factors is depicted schematically in Figure 2.[3] The electron transfer pathway in photosynthesis begins with photon absorption by the reaction center chlorophyll, P_{680}, leading to a charge separation that produces $P_{680}^{+}Q_A^{-}$. The quinone, Q_A, reduces another quinone Q_B. Following two photochemical events, this quinone is released from the membrane and the electrons are transported to PS I. On the oxidizing side of PS II, a complex containing the transition metal manganese, upon oxidation, provides electrons for a tyrosine molecule which in turn reduces P_{680}^{+}. This pathway will be described in more detail below.

The PS II/OEC contains both extrinsic and intrinsic polypeptides as well as a number of enzymatically active co-factors (the kinetics of the electron transfer reactions associated with these will be discussed in the following section). There are three extrinsic polypeptides, identifiable by their molecular weights: the 17, 23, and 33 kDa polypeptides. These serve several purposes. First, the 33 kDa protein protects the manganese complex associated with water oxidation. This Mn ensemble is maintained in a configuration that optimizes oxygen evolution by this polypeptide. The 33 kDa polypeptide binds directly to the intrinsic polypeptides, an interaction further stabilized by the Mn complex.[4] Recent crosslinking studies have determined the stoichiometry of this polypeptide to be 1:1 with an intrinsic polypeptide (the 47 kDa).[5] The 33 kDa protein also serves an additional function; it isolates the redox active species involved in water oxidation from the aqueous environment.[4] This is an important function in that the water oxidizing system is susceptible to spurious reductants and this biochemical barrier provides a redox shield that allows it to perform its water splitting function successfully. Unfortunately, this polypeptide is difficult to study quantitatively due to the

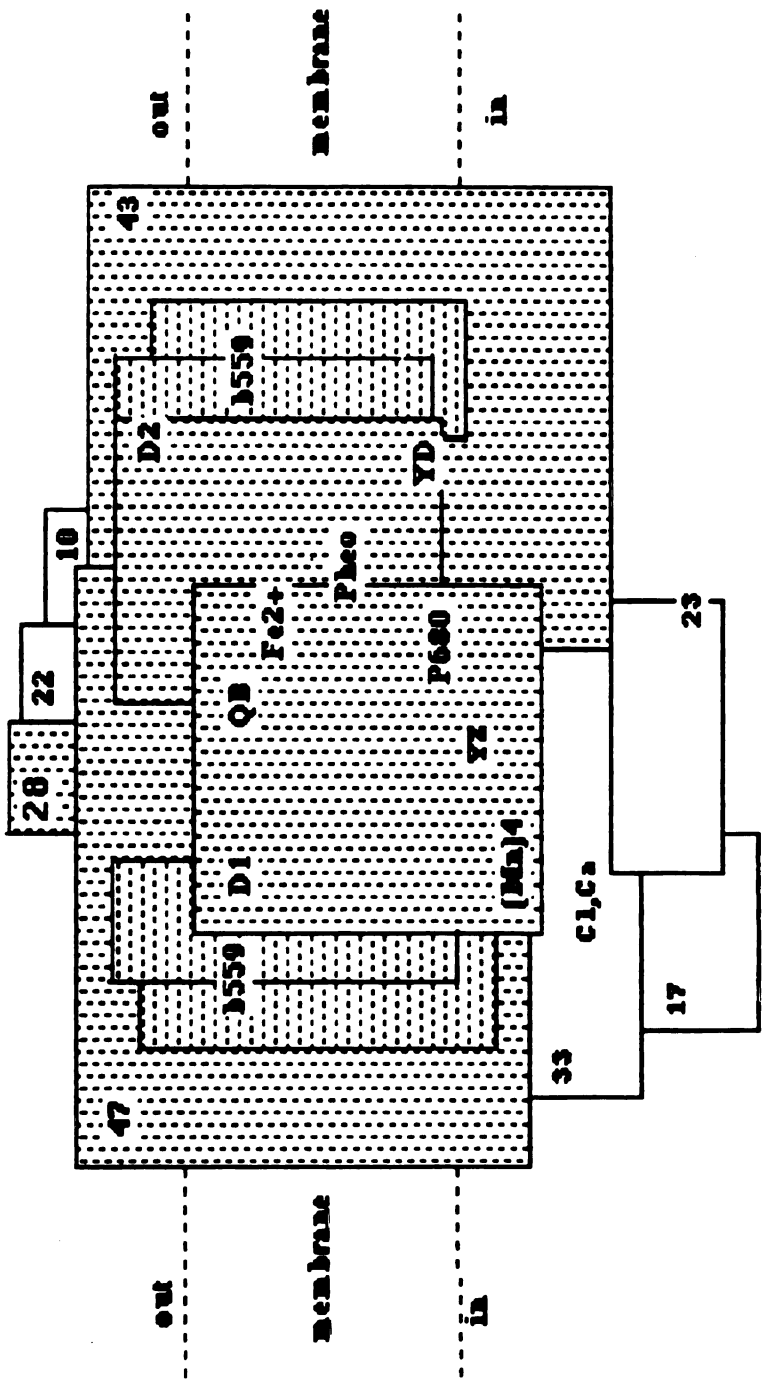

Figure 2: Proposed structure of the PS II/OEC including polypeptides and co-factors.

rearrangements of the intrinsic polypeptide core that occur upon removal of these soluble subunits.[6] Extraction methods and their effect on the PS II/OEC will be discussed in an upcoming section.

The remaining extrinsic polypeptides, the 17 and 23 kDa proteins, also function in binding co-factors needed for water splitting chemistry, in particular the calcium ion and the chloride ion. These two polypeptides also protect the manganese ensemble from exogenous reductants.[4] Upon removal of the 17 and 23, oxygen evolution can only be maintained with increased concentrations of both calcium and chloride.[7]

The photochemical core of PS II is formed by two membrane spanning intrinsic polypeptides. These heterodimers (MW approximately 32 kDa) , commonly known as D1 and D2, bind chlorophylls, pheophytins and quinones that mediate the light driven charge separation reactions.[8] Sequence and functional homologies between the L and M subunits of the bacterial reaction center from *Rhodopseudomonas viridis* and the D1/D2 heterodimer have led to the suggestion that D1 and D2 each contain five membrane spanning helices.[9-10] This structural arrangement leads to a pseudo-C_2 symmetry for the PS II/OEC. This apparent symmetry is very useful in designing experiments to study the PS II/OEC.[11] However, this symmetry is broken by the incorporation of the manganese ensemble which, in one proposed model , is located off of the C_2 symmetry axis.[12] The controversy surrounding the organization and location of the manganese complex will be discussed in a later section.

The remaining intrinsic polypeptides have a wide variety of functions. By providing binding sites for accessory chlorophylls the 43 and 47 kDa proteins have mainly a light harvesting function. The 23 kDa polypeptide can be isolated in its pure form, and in addition to binding chlorophyll a, has been implicated in maintaining the Q_B site on D1.[13-14] Conformational changes to D1 are modulated depending on whether this quinone-binding site is occupied. The smaller (22 and 10 kDa) polypeptides do not have binding sites for any of the co-factors. However, removal of these two proteins

results in increased accessibility of exogenous acceptors like DCBQ to Q_A^-. Therefore, the 22 and 10 kDa proteins must, in some way, influence the environment around these quinones. The final two intrinsic polypeptides (4 and 9 kDa MW) each provide a single histidine ligand to the heme of cytochrome b_{559}.[15]

Electron Transfer in Photosynthesis

The initial step in photosynthesis occurs when a photon of light is absorbed by a light harvesting protein antenna complex (called the LHC) composed of non-covalently bound chlorophyll a, chlorophyll b and carotenoid molecules (in higher plants and green algae). In cyanobacteria, this antenna complex is the phycobilisome. These antenna pigments then transfer energy via exiton interaction and Forster transfer to the reaction centers. All of the energy absorbed by the LHC is transferred to a specialized monomer or dimer of chlorophyll a in PS II known as P_{680}. This name is derived from the absorption maximum of this molecule at 680 nm. This energy promotes the P_{680} molecule into an excited singlet state. This excited state within 3 picoseconds, reduces a nearby pheophytin molecule (Pheo), forming $Pheo^-$ and P_{680}^+. To prevent recombination, the $Pheo^-$ quickly (within 300-600 ps) reduces a nearby plastoquinone, Q_A.[16]

The electrons are shuttled out of PS II by electron transfer from Q_A^- to another plastoquinone, Q_B in about 200 μs. An interesting change occurs at this point. Previously, the photosynthetic process had been composed of single electron events. The movement of electrons out of PS II, however, is a multielectron process. Q_B^- remains tightly bound in its binding site until a *second* photochemical event reduces it to Q_B^{2-} whereupon it becomes protonated and is released from its binding site as plastoquinol. The plastoquinol is then oxidized by cytochrome b_6f and the electrons are transported to PS I by a plastocyanin molecule. The Q_BH_2 is replaced in its binding site by an oxidized quinone from the membrane associated quinone pool.[17]

Recombination between P_{680}^+ and Q_A^- (which occurs with a half time of approximately 100 μs) would be a photosynthetically "wasteful" process. To prevent this recombination, either Q_A^- must be oxidized or P_{680}^+ reduced in a time considerably shorter. The electron transfer between Q_A^- and Q_B has been measured to be in the 100-500 μs time range.[17] This indicates that the reduction of P_{680}^+ must occur in the submicrosecond time range. The reduction, however, was found by Witt and coworkers to depend on the state of the OEC.[18] To explain this dependence, a redox active donor was postulated. This donor operates as a charge transfer interface between the OEC and P_{680}^+ in an equilibrium that depends on the net charge of the OEC.[18] There has been spectroscopic evidence for this donor, a tyrosine residue (Y_Z), although under non-physiological conditions other complexes may donate to P_{680}^+.[19] The oxidizing power generated in producing P_{680}^+ must be directed eventually at water. Tyrosine oxidation, producing the highly oxidizing (E_m^0=1.0 V) Y_Z^+ radical is a means by which to achieve this.[19]

There is a second redox active tyrosine in PS II known as Y_D^+. It has been identified as Tyr-161 of the D2 polypeptide by site directed mutagenesis experiments.[20] It has no known function and in its oxidized form is responsible for the dark stable EPR signal known as Signal II.[19] The EPR lineshapes of Y_D^+ and Y_Z^+ are identical which indicates that the unpaired spin density distribution and the orientation of the tyrosine phenol ring with respect to the polypeptide backbone are identical for both species.[21] However, Y_D^+ is not involved in the electron transfer reactions that lead to water oxidation. This was confirmed with site-directed mutagenesis experiments by Debus et al where phenylalanine was substituted for both Y_Z and Y_D.[20] In the Y_Z case, photosynthetic growth was absent after the deletion whereas in the Y_D case photosynthetic growth continued. The two tyrosine moieties are related by an apparent C_2 symmetry. These symmetry related branches, however, are not related *functionally*.

The Oxygen Evolving Complex

The OEC is the site of water oxidation in the photosynthetic process. The half reaction corresponding to this process,

$$2\ H_2O \text{ -------> } O_2 + 4\ H^+ + 4\ e^-$$

has an average reduction potential of 0.93 V at pH=5.0.[26] The energy required to drive this reaction comes from the oxidized P_{680}. The midpoint potential for this reaction

$$P_{680} \text{ -------> } P_{680}^+ + e^-$$

is 1.17 V at pH=5.0.[22] The stoichiometries of these two reactions bring up an interesting mechanistic question. A single absorbed photon generates only one oxidizing equivalent, however the water splitting process is a four electron process. The oxidizing power of four photons needs to be combined in order to facilitate water oxidation. Insight into the resolution of this paradox began with the now classic O_2 flash yield measurements of Joliot and co-workers.[23] These experiments showed that the O_2 produced by a sequence of brief (about 10 μs) saturating light flashes showed a damped oscillatory pattern with a periodicity of four following the third flash. These data were soon reproduced by Kok and co-workers and a working kinetic model was established.[24] This model showed that the PS II units function independently in accumulating the four oxidizing equivalents necessary to split water. This so-called S-state cycle is driven by successive photoactivations of PS II. A schematic representation of this cycle is shown in Figure 3. The S represents the water splitting center and the subscripts indicate the number of oxidizing equivalents accumulated. Oxygen evolution occurs only after the S_4 state has been achieved. This model accurately explains the details of the flash experiments. Maximal oxygen evolution occurs after the third flash with repeated maxima after successive four flash intervals. See Figure 4 for similar data on spinach chloroplasts by Babcock.[25] The oxygen evolution vs. flash pattern eventually dephases and reaches a steady state value. This pattern can be explained if both S_0 and S_1 are dark stable states. After dark adapting samples it was found that approximately 60% of the centers were in

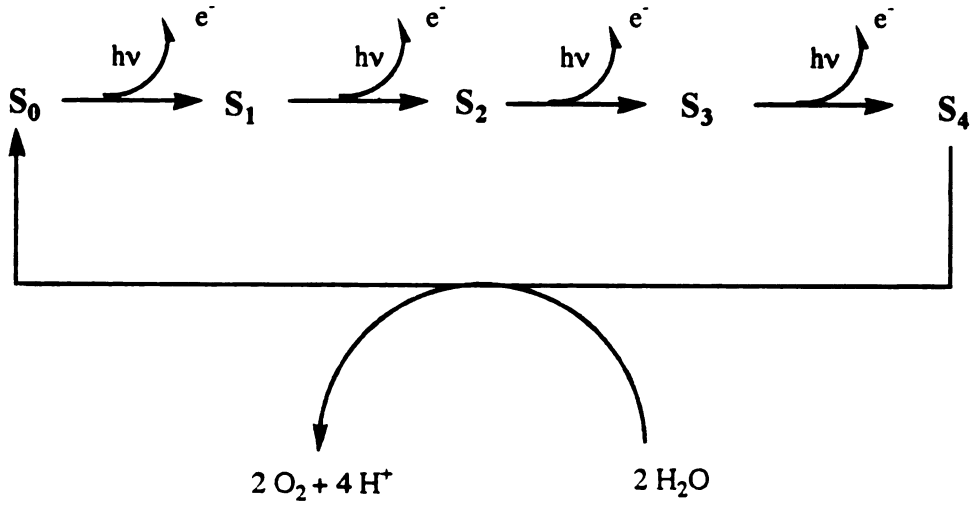

Figure 3: Kok's S-state cycle

S_1. To concentrate the OEC in S_2 further, Kok and co-workers took dark adapted samples, subjected them to a brief flash and allowed them to dark adapt a second time. This treatment resulted in almost no oxygen evolution after the first two flashes and an even larger maximum after the third.[24] The slow dephasing seen is due to the non-zero probability of "misses" and "double hits" resulting in the loss of S-state coherence.

Manganese

The first row transition metal manganese has long been associated with the oxygen evolving complex of photosynthesis. Its many stable oxidation states (+2 to +7) make it an ideal metal center for the multielectron chemistry that occurs in the OEC.[26] The earliest experiments linking Mn to oxygen evolution were performed in the 1930's and showed that algae grown on low levels of manganese exhibited a decreased ability to evolve oxygen.[27] Later experiments placed the location of manganese directly in PS II. Cheniae and Martin, using heat shock techniques, demonstrated a loss of oxygen evolution concomitant with the release of Mn.[28] Yocum and co-workers found the major fraction of Mn^{2+} in highly oxygen evolving thylakoid membranes was in an EPR silent form.[29] This amount, calculated to be 4 per 400 chlorophyll, was resistant to release by Ca^{2+} and was released by using acidification processes and subsequently quantified with EPR measurements. A stoichiometry of four Mn per PS II was determined for optimum functioning of photosynthetic oxygen evolution. The organization and corresponding valence states of this manganese ensemble are not known and are currently the subject of much debate among researchers. Dimers, trimers and tetramers have all been suggested as structures for this multinuclear cluster.

A variety of techniques have been employed to determine the oxidation state changes of this functional Mn ensemble that correspond to S-state transitions.

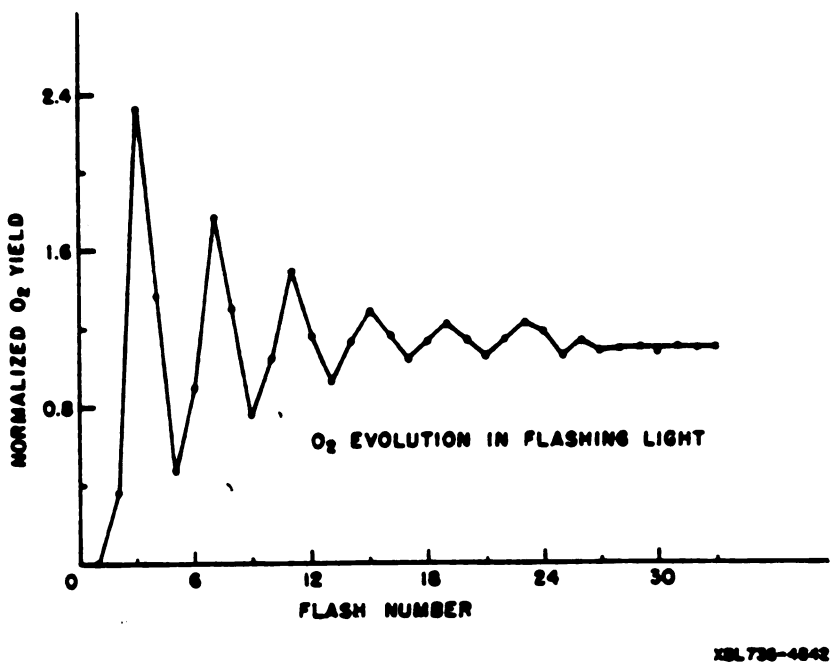

Figure 4: Oxygen evolution as a function of flash number (from reference 25).

EXAFS: The earliest spectroscopic results were reported by Kirby et al in 1981.[30] Manganese X-ray absorption fine structure (XAFS) results for wild type chloroplasts and chloroplasts treated with alkaline Tris buffers to release Mn and inactivate the water splitting mechanism were recorded. The differences between these, representing the active pool of Mn, were shown to be similar to the XAFS from model di-μ-oxo-bridged Mn systems. Later, using a biochemically refined preparation, Yachandra et al [31] presented extended XAFS (EXAFS) data showing Mn-Mn distances of 2.7 A. This proximity provides evidence for at least a binuclear Mn cluster. The EXAFS data also included a Mn-nitrogen or oxygen distance of 1.75-1.8 A and a disordered shell of oxygens or nitrogens at an average distance of 2.15 A from the Mn. A disadvantage of using EXAFS as an analytical tool is the uncertainty in the atomic number determination of ligands coordinated to the metals. This uncertainty ($\pm$ 10 for atomic number) results in an ambiguity in ligation as far as nitrogen and oxygen are concerned, two proposed ligands to the Mn ensemble.[32] Recent work by Penner-Hahn in which both improved preparations (concentration of Mn approximately 1.5 mM) and higher detection efficiency were used, confirmed two to three Mn-Mn distances of 2.7 A.[32] An additional third backscattering shell of 3.3 A which includes Mn was also confirmed. Again, this provides evidence for a multinuclear (trimer or tetramer) cluster.

EPR: Perhaps the greatest amount of information regarding the structure of the Mn ensemble has come from magnetic resonance techniques, particularly electron paramagnetic resonance (EPR). EPR can be used to identify paramagnetic species and to characterize the environment around them. The Mn ensemble in the oxygen evolving complex is a system which, through the S-states, generates a number of paramagnetic intermediates, thus making it ideal for analysis by EPR. Both continuous wave (cw) and

pulsed EPR techniques have been employed to characterize the structure of and ligands to the Mn ensemble.

The first EPR signal associated with the Mn ensemble was reported by Dismukes and Siderer in 1980.[33-34] This so-called multiline signal was initially observed in samples that had been rapidly frozen following a flash of light at room temperature. The EPR signal consists of 18-20 hyperfine lines separated by 85-90 gauss, is centered at g=1.982 ± 0.002 and has a linewidth of 1500-1800 gauss, see Figure 5. It can only be observed at temperatures less than 35 K. The signal amplitude oscillates with flash number having maximal intensity after the first and fifth flashes. This flash induced periodicity is analogous to the oscillations seen byJoliot[23] and Kok[24] in the S-state experiments. The multiline signal was thus attributed to the S_2 state of the Kok cycle. This was confirmed with temperature dependent decay experiments performed by Brudvig et al.[35] The decay rate following flash illumination was found to be temperature dependent. The half-time decay of 40 s at 295 K contrasts markedly with the half-time decay of 40 min at 253 K. Below 240 K a single illuminating flash becomes less likely to produce the multiline signal. The 40 s half-time in particular provides evidence that the multiline spectrum results from a relatively stable state rather than a transient intermediate. This 40 s decay is very similar to that reported for the S_2 state of the PS II/OEC.[36-37]

The advancement of the S states was also found to be markedly temperature dependent; S_1----->S_2 can occur at temperatures as low as 160 K and S_2----->S_3 occurs readily only at temperatures above 210 K. Brudvig and co-workers found that a single intense flash of light became progressively less effective in generating the multiline signal at temperatures below 240 K and, at lower temperatures (160 K), continuous illumination was needed.[35]

Model compounds: Attempts at reproducing the multiline spectrum using synthetic model compounds have been numerous. The oxo-bridged dimer

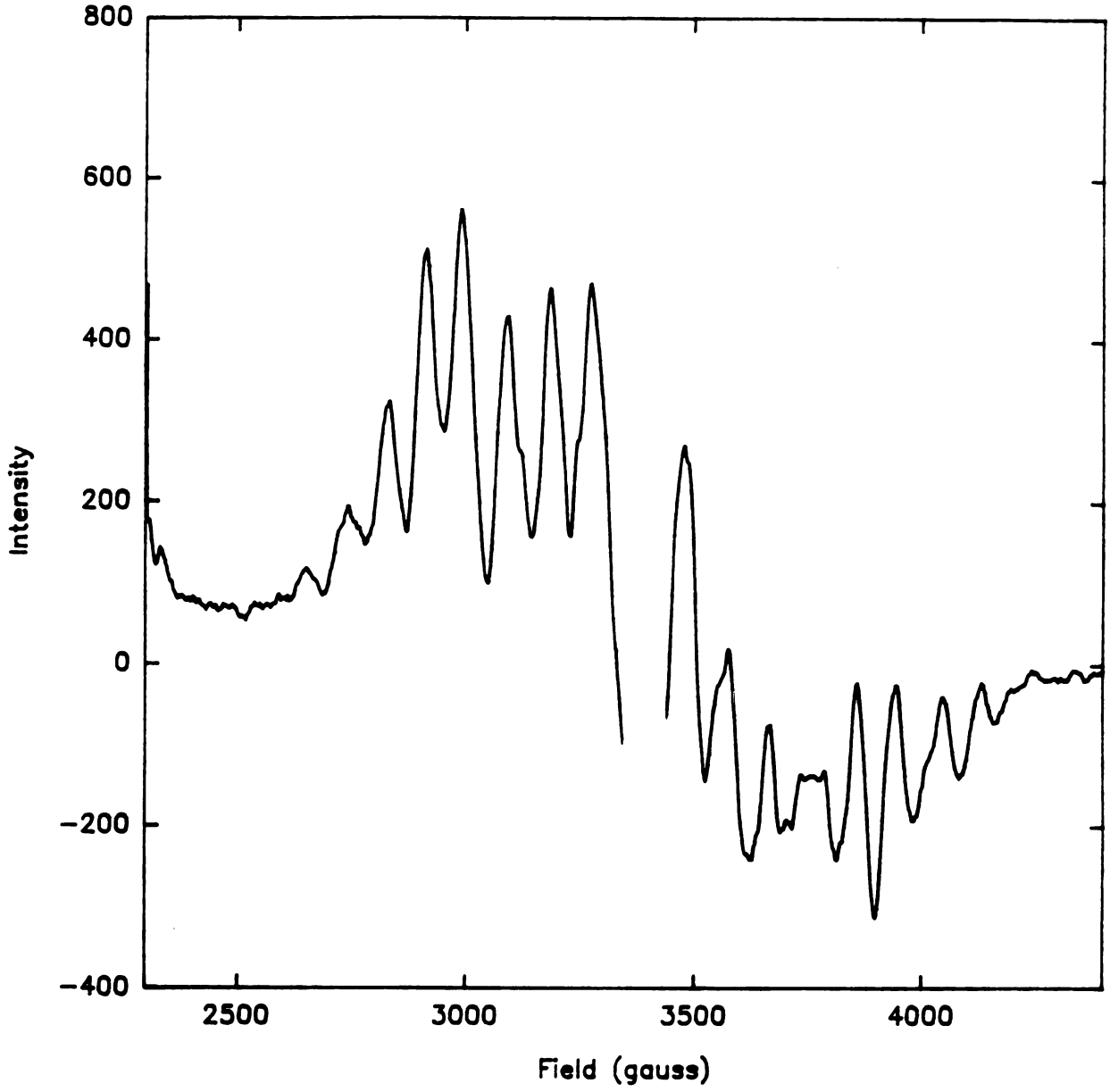

Figure 5: The multiline spectrum associated with the S_2 state of the OEC.

$[Mn^{III}Mn^{IV}(O)_2(bpy)_4]^{3+}$ has been extensively studied as a model for the Mn cluster in the OEC. The similarity of the EPR spectrum to that of the multiline led early researchers to the theory that the multiline originated from a mixed-valence, exchange-coupled cluster of Mn ions. Unfortunately, these strongly coupled dimers did not exhibit any EPR features beyond the 16 line spectrum expected for an S=1/2 ground state.[30] Recently, an asymmetric $Mn^{III}Mn^{IV}$ dimer has been synthesized; it exhibits the weak antiferromagnetic coupling and the reversible thermally regulated transition from an S=1/2 ground state to an S=3/2 excited state thought to occur in the Mn complex.[38] The EPR signal from this compound looks similar to that obtained from the Mn complex.

Trinuclear compounds have also been postulated as models for the OEC Mn complex. The EPR spectra of two of these compounds:

$Mn_3(dien)_3(OAc)_2(ClO_4)_3O_3 \cdot H_2O$ (A)

$Mn_3(dien)_3(OAc)_2I_3O_3H_2O \cdot 0.33\ CH_3OH$ (B)

exhibit the 16 line hyperfine coupling indicative of an effective S=1/2 ground state.[39]

The evidence for a tetranuclear Mn ensemble has also been convincing. Dismukes et al using EPR simulations, have postulated that a tetramer composed of three Mn (III) and one Mn (IV) could model the multiline spectrum.[40] This simulation, however, failed to reproduce the breadth and the number of lines in the experimental spectrum. Recent theoretical studies have provided additional evidence for a tetramer.[41] By using six fitting parameters, the shape of the experimental spectrum and its hyperfine pattern,splittings and relative intensities have been described. However, the parameters used do not give direct information regarding the structure of the tetramer nor do they provide any information about the coupling schemes between the ions.

Isolation and Characterization: Although the nuclearity of the Mn ensemble remains unclear, information regarding function and structure can be obtained from characterization of the environment around the manganese. Improved biochemical

preparations and subsequent magnetic resonance analysis have yielded much information about co-factors and ligands to the OEC.

The role of calcium in PS II has been well documented. Initially observed in photosynthetic membranes from cyanobacteria calcium requirements have played roles in higher plant photosynthesis as well.[42] Reconstitution of calcium depleted membranes was found to reverse the inhibition of oxygen evolution.[43] Depletion of calcium can be accomplished by salt washing either in the light or dark with 1-2 M NaCl. This treatment removes the 17 and 23 kDa polypeptides and allows access to the proposed calcium site. Salt washing in the light is facilitated by the addition of a chelating agent such as ethylene diamine tetraacetic acid (EDTA). Because illumination was found to have an effect upon the ease of calcium extraction, the role of calcium in PS II was associated with the S-states of the OEC. The ease of extraction progresses in the order $S_3 > S_2 \sim S_0 > S_1$.

Calcium effects: The multiline spectrum has been studied to determine the effect of calcium depletion upon S-state turnover. The S-state transition inhibited by calcium depletion has been controversial. Boussac and Rutherford provide evidence for blockage of the S_3------> S_0 transition in NaCl washed samples.[44] Continuous illumination of the calcium depleted samples at 200 K resulted in a normal S_2 multiline signal. The intensity of this signal was comparable in amplitude to the signal from calcium reconstituted samples. Flash experiments showed normal multiline formation upon the first flash with a typical decrease in amplitude after the second flash. However, no increase in intensity was observed upon the fifth flash. The typical S-state oscillation pattern was present upon calcium reconstitution of these samples.

Strontium effects: Reconstitution of these samples using Sr^{2+} instead of Ca^{2+} gave a modified multiline signal.[45] The Sr^{2+} reconstitution resulted in losses, splits, shifts and

redistributions of the hyperfine lines. The average hyperfine spacing decreased from 87.9 G in the Ca^{2+} reconstituted samples to 71.0 G in the Sr^{2+} samples. This indicates that the introduction of Sr^{2+} into the calcium site perturbs the Mn cluster such that a slight conformational change occurs.

Chelator effects: Chelator concentration during salt washing also has an effect upon the multiline spectrum.[46] High concentrations of chelator (10 mM) lead to a dark stable, markedly modified multiline signal. Direct binding of the carboxylic acid functional groups of the chelator to the Mn is one possible explanation for the modifications observed in the multiline spectrum. This ligation is not possible in the presence of Ca^{2+} which provides evidence that Ca^{2+} may regulate access of a ligand to a binding site on the Mn.

Nitrogen ligation: Nitrogen, particularly the nitrogen moiety of the amino acid histidine, has been postulated as a potential ligand to the Mn complex. EPR studies of spinach grown hydroponically with $K^{15}NO_3$ as the sole nitrogen source were done in 1989 in an attempt to resolve the nitrogen ligation question.[47] There were no observable changes in either the general shape or the linewidth of the hyperfine structure of the multiline spectrum. The fine structure was therefore attributed to manganese hyperfine interactions and not to nitrogen superhyperfine couplings.

ESEEM Characterization: Often in EPR, and particularly with transition metal complexes, the magnitude of the superhyperfine interactions is small compared to the overall linewidth of the signal. To resolve these couplings better, other techniques must be used. For large hyperfine interactions, double resonance techniques such as ENDOR (electron nuclear double resonance) can be applied. The resolution of smaller hyperfine couplings can be accomplished by using spin echo techniques.

Electron spin echo envelope modulation (ESEEM) techniques were used to observe nitrogen interactions between the Mn complex and a proposed histidine ligand in both cyanobacteria and spinach thylakoid preparations.[48-49] By studying ammonia inhibition mechanisms in PS II, Britt and co-workers were able to identify hyperfine and quadrupole frequencies associated with the ^{14}N (I=1) of ammonia. Subsequent isotopic exchange experiments with ^{15}N (I=1/2) were used to confirm the nitrogen from ammonia as the source of these frequencies. Analogous experiments were performed on oxygen evolving cyanobacteria preparations. Cultures of the cyanobacteria *Synechococcus* were grown with KNO_3 as their only source of nitrogen. Again, hyperfine and quadrupole frequencies were determined using ESEEM spectroscopy. Isotope labelling experiments confirmed nitrogen as the origin of these frequencies.[49]

Chapter 2
Magnetic Resonance Theory

EPR: Electron paramagnetic resonance techniques are useful in identifying the paramagnetic species present in a sample. Interactions between a paramagnet and nearby magnetic nuclei can also be characterized by using this technique. As previously mentioned, both cw and pulsed EPR techniques have been used on the photosynthetic system to characterize the ligand environment around the Mn ensemble. Conventional cwEPR has not been able to account completely for the splittings seen in the multiline spectrum. In this section, the theory behind cw and pulsed EPR and its application to the multiline spectrum will be discussed.

An EPR spectrum can be described with a spin hamiltonian composed of several terms, each describing the interaction of the unpaired electron with its environment.[50] This hamiltonian, can be written as

$$\mathcal{H} = H_{EZ} + H_{NZ} + H_{HF} + H_{EI} \qquad (1)$$

where H_{EZ} represents the electronic Zeeman hamiltonian, H_{NZ} the nuclear Zeeman hamiltonian, H_{HF} the isotropic hyperfine hamiltonian, and H_{EI} the exchange interaction hamiltonian. The hamiltonian operates on the spin only part of the total wavefunction.

The first term of equation 1 represents the interaction of the unpaired electron with the applied magnetic field. The Zeeman hamiltonian can be explicitly written as

$$H_{EZ} = g\beta HS \qquad (2)$$

where g is the isotropic electronic g factor, β the Bohr magneton, H the applied magnetic field and S the spin angular momentum operator. The effect of this term is to split the degeneracy of the two spin only wavefunctions for the electron (S=1/2 where S in this context is total spin). The energy corresponding to these levels is given by

$$E = g\beta HM_S \qquad (3)$$

where M_S represents the quantum number associated with the specific spin state. For a system with a single unpaired electron, M_S can have two values, $\pm 1/2$. This gives an energy separation of

$$\Delta E = E_2 - E_1 \tag{4a}$$

$$\Delta E = g\beta H \tag{4b}$$

Transitions between these two energy levels (Zeeman levels) can be induced by an electromagnetic field of frequency ν if the energy of an incident photon, $h\nu$, is equal to the splitting between levels. These transitions between energy levels are the resonances present in an EPR spectrum. The resonance condition for EPR is given in equation 5.

$$h\nu = g\beta H \tag{5}$$

As can be seen from this expression the energy separation depends on both the field and frequency values. EPR experiments are performed by holding the frequency constant while varying the magnetic field. Therefore, the energy separation increases as the field becomes larger. This is evident in the energy level diagram for an S=1/2, I=1/2 system as presented in Figure 6.

The magnetic field also has an effect on magnetic nuclei. The second term in equation 1, the nuclear Zeeman interaction, represents the interaction between the nuclear spin and the applied Zeeman field. It is given explicitly by equation 6:

$$H_{NZ} = - g_n \beta_n H I \tag{6}$$

where g_n is the nuclear g factor, β_n the nuclear magneton, and I the nuclear spin angular momentum operator. By applying the field along the z axis and assuming quantization of the nuclear spin along that axis, the nuclear spin quantum number M_I can be substituted in the corresponding energy expression giving

$$E = - g_n \beta_n H M_I \tag{7}$$

The effect of this interaction is apparent in the energy level diagram in Figure 6.

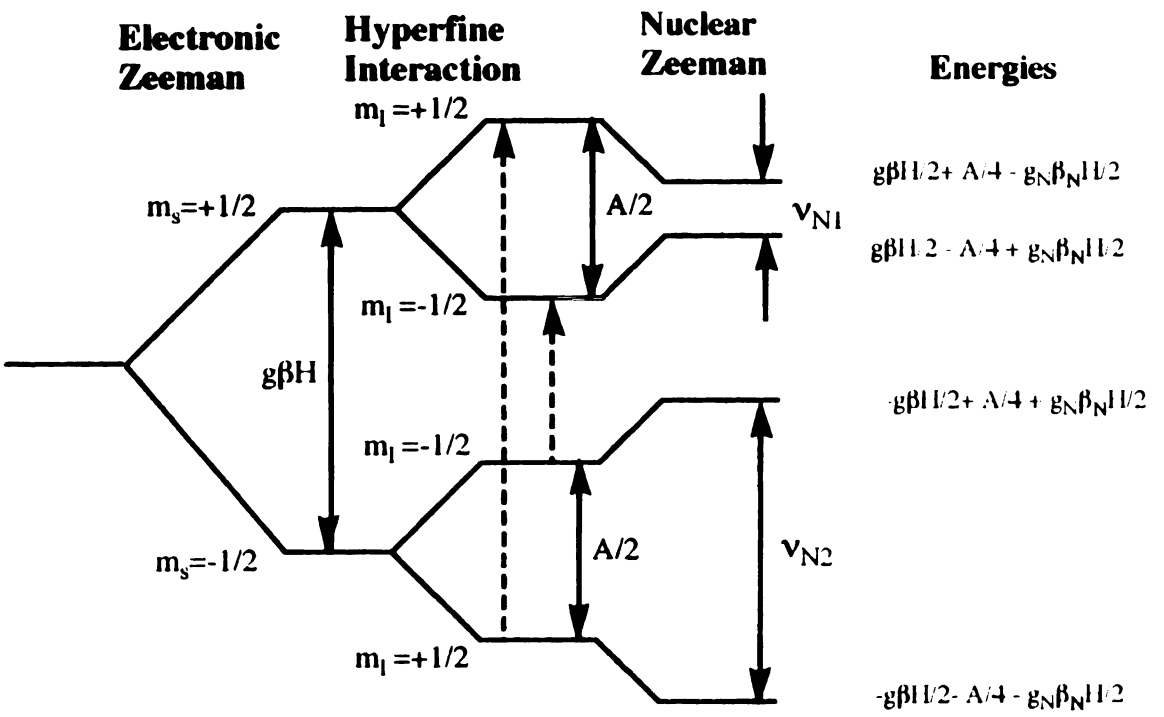

Figure 6: Energy level diagram for an S=1/2, I=1/2 system. The dashed lines represent allowed EPR transitions corresponding to the selection rules $\Delta M_s = \pm 1$ and $\Delta M_I = 0$. The solid lines represent energy differences between the states. The corresponding energies are given on the left.

The magnetic field felt by the unpaired electron is a combination of the applied field and the fields due to nearby magnetic nuclei (I>0). The third term in the hamiltonian from equation 1 represents the interaction of the electron with nearby magnetic nuclei and is termed the hyperfine coupling. The hamiltonian for this interaction can be given by

$$H_{HF} = hA_o \, \mathbf{S} \cdot \mathbf{I} \qquad (8)$$

The z components of the electronic and nuclear spin angular momentum operators can be substituted in place of $\mathbf{S} \cdot \mathbf{I}$ providing the hyperfine interaction is less than the electronic Zeeman interaction. There are two components to this hyperfine term. The first, termed isotropic, is represented by equation 8. It results from Fermi contact coupling, is orientationally independent, and originates from the non-zero probability of the electron being located at the nucleus of the coupled atom. This can only occur if the unpaired spin density resides in an s orbital. This interaction energy was given by Fermi as

$$E_{iso} = -(8\pi/3) \, |\psi(0)|^2 \, \mu_{ez} \, \mu_{nz} \qquad (9)$$

where $\psi(0)$ is the wavefunction evaluated at the nucleus and μ_{ez} and μ_{nz} are the magnetic dipole moments of the electron and the nucleus, respectively. Substitution of the nuclear and spin angular momentum operator relations for the classical magnetic dipole moments in equation 9 will yield the isotropic hyperfine hamiltonian. The term hA_o represents the interaction energy between the electron and the nucleus and is equal to $(8\pi/3)g_n\beta_n g_e\beta_e|\psi(0)|^2$. A_o is called the hyperfine coupling constant and is measured in units of gauss or megahertz. The energy corresponding to this interaction can then be given as

$$E = hA_o M_S M_I \qquad (10)$$

For an S=1/2, I=1/2 system these energies are:

$$E_{1/2,1/2} = hA_o/4 \qquad (10a)$$

$$E_{1/2,-1/2} = -hA_o/4 \quad (10b)$$

$$E_{-1/2,1/2} = -hA_o/4 \quad (10c)$$

$$E_{-1/2,-1/2} = hA_o/4 \quad (10d)$$

The effect of this interaction on the energy levels can be seen in Figure 6.

The second part of the hyperfine interaction is the orientationally dependent dipolar coupling. The dipolar coupling is a through space interaction between the unpaired electron and neighboring nuclei. The dipolar coupling is anisotropic and described by the tensor A given in equation 11. The magnitude of the hyperfine tensor A is dependent on the orientation of the Zeeman field relative to the A-tensor axis system.

$$A_{HF} = A_{iso} + A_{dipolar}$$

$$A_{dipolar} = \mathbf{S} \cdot \mathbf{A}^T \cdot \mathbf{I} \quad (11)$$

The hyperfine coupling in the Mn complex has been found to be primarily isotropic, therefore this dipolar part of the hamiltonian can be neglected.

Referring again to Figure 6, the allowed transitions in an EPR experiment correspond to the selection rules $\Delta M_S = \pm 1$ and $\Delta M_I = 0$. These transitions can be seen in Figure 6.

The fourth term in the hamiltonian, the exchange coupling term H_{EI}, arises as a result of the linkage of two molecular fragments, each containing unpaired electrons.[51] The magnitude of this exchange interaction depends on the bonding characteristics of the two metal centers. Direct metal-metal bonds result in extremely large couplings. However, moderate to high oxidation state manganese compounds rarely form metal-metal bonds. For these types of compounds, a super exchange pathway mediates the magnetic interaction.

The effective spin on a mixed valent complex results from interactions between the two fragments. Symmetry requirements constrain electrons on adjacent atoms such that they can occupy the same space only if their spins are antiparallel. An important result of this constraint is the phenomenon of antiferromagnetic coupling. Consider an

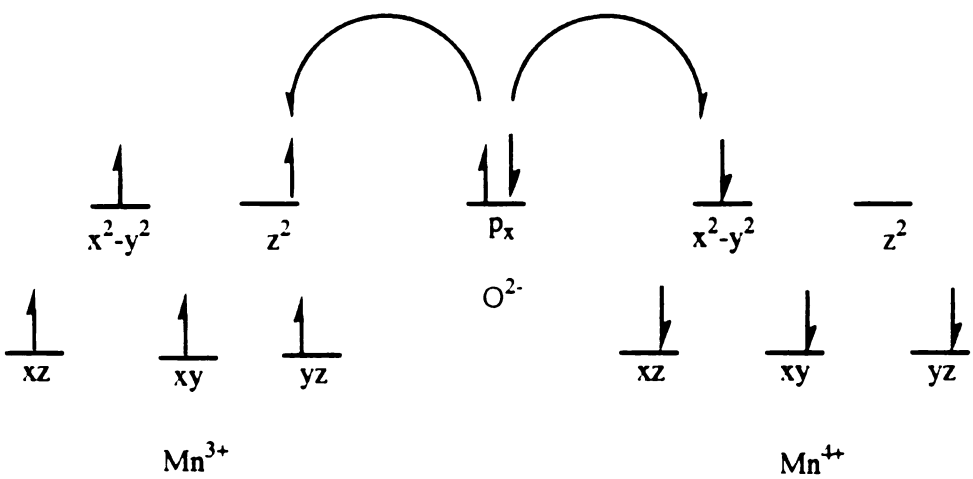

Figure 7: Schematic representation of antiferromagnetic coupling in the fragment Mn^{3+}- O^{2-}- Mn^{4+}.

M-L-M compound in which p electrons from the ligand overlap with d electrons from the metal to form the M-L bonds.[51] Figure 7 shows an Mn^{3+}-O^{2-}-Mn^{4+} fragment which illustrates this. The formation of a bond between the Mn^{3+} and the O requires partial transfer of an electron from the p_x oxygen orbital into the $d_{x^2-y^2}$ orbital of the Mn. The Pauli principle constrains the electron such that this electron must be anti-parallel to the electrons in the Mn orbitals. The remaining electron from the oxygen is partially transferred into the $d_{x^2-y^2}$ orbital of the Mn^{4+}. The anti-parallel configuration of the two electrons from the ligand must be maintained during this transfer. In order to accommodate the Pauli principle, the electrons in the Mn^{4+} must flip, creating a coupling of electron spins of the two manganese atoms so that they are anti-parallel to one another. This results in an effective spin of 1/2 for the system. The strength of the exchange interaction (J) is usually small compared to bonding energies, but large compared to the energies associated with the magnetic properties of the electron. The presence of antiferromagnetic coupling therefore, results in substantial modifications of quantities associated with electron magnetism, particularly EPR. These modifications are accounted for in the exchange interaction term of the hamiltonian.

The spin hamiltonian for exchange interaction is given by[50]

$$H_{EI}=g\beta H\,(S_{1z}+S_{2z})+hA_o(S_{1z}I_{1z}+S_{2z}I_{2z})+hJ\,\mathbf{S_1}\cdot\mathbf{S_2} \qquad (12)$$

where $\mathbf{S_1}$ and $\mathbf{S_2}$ represent the spin operators for electrons 1 and 2 and J is the exchange integral defined by

$$J=h^{-1}\langle\phi_A(1)\phi_B(2)\,|\,(e^2/r_{12})\,|\,\phi_B(1)\phi_A(2)\rangle. \qquad (13)$$

Here ϕ_A is the one-electron orbital on fragment A , ϕ_B is the one-electron orbital on fragment B, and r_{12} is the separation of electrons 1 and 2. The corresponding energies can be obtained from this hamiltonian. For the case $|J| >> |A_o|$, the hyperfine term in equation 12 can be eliminated. The set of eigenvalues for this zero order hamiltonian are

$$E_{1,1} = g\beta H + hJ/4 \qquad (14a)$$

$$E_{1,0} = + hJ/4 \qquad (14b)$$

$$E_{1,-1} = -g\beta H + hJ/4 \qquad (14c)$$

$$E_{0,0} = -3\ hJ/4 \qquad (14d)$$

where the subscripts indicate the states S^2 and S_Z. These energies are plotted in Figure 8 for J>0.

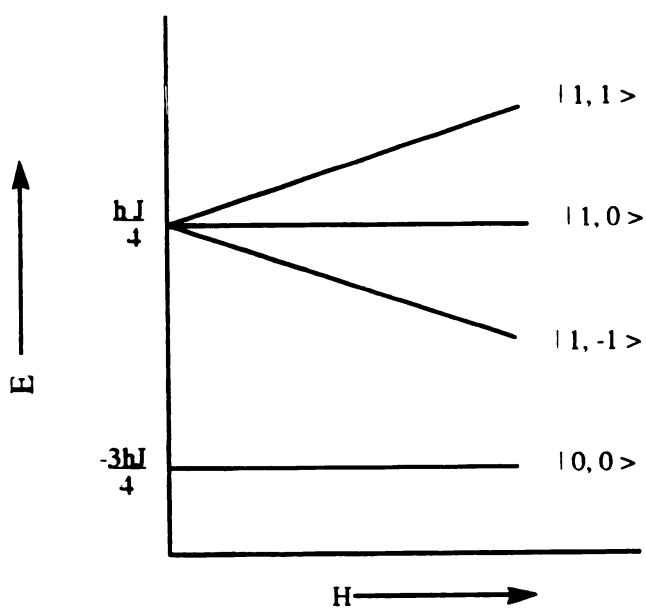

Figure 8: The effect of exchange coupling on the triplet and singlet states of an S_1=1/2, S_2=1/2 system. The degeneracy at zero field is removed upon the exchange interaction.

ESEEM: Electron spin echo envelope modulation (ESEEM) is a sensitive technique for measuring the small superhyperfine couplings in systems with large inhomogeneously broadened EPR lines. Inhomogeneity in an EPR line results from the interaction of the unpaired electron with varying local fields.[50] This variation can be due to anisotropy in either the g or A terms of the hamiltonian. The electron is subjected to slightly different local fields such that only a small fraction of the spins are in resonance at a given time. The EPR spectrum is then composed of a superpostion of these "spin packets" (Figure 9). Inhomogeneous broadening can also be the result of unresolved hyperfine interactions. A large number of hyperfine components leads to a decrease in spectral resolution.[50] These large interactions can be resolved using double resonance techniques like ENDOR. A less common cause of inhomogeneous broadening is inhomogeneity in the applied magnetic field, although this becomes a problem only at large field values. Pulsed EPR techniques can resolve the structure within a single spin packet by effecting large rotations of net electron spin magnetization.

Two pulse ESEEM experiment: To explain the theory behind a 2 pulse ESEEM experiment effectively, a rotating coordinate system will be used. As depicted in Figure 10, this coordinate system is rotating with frequency ω_0 and its axes are denoted with a prime superscript (e.g. X', Y', Z').[52] The applied magnetic field, H_0, is along the Z axis and detection is along the Y axis.

Consider two spin packets with characteristic Larmor frequencies ω_i and ω_j (see inset, Figure 10) which differ from the frequency of the rotating frame. Each of these spin packets can be considered independently from the others. At thermal equilibrium there is a net magnetization, M_{total}, along the z axis due to the sum of the individual magnetic moments of the electrons (see Figure 10a). A short, intense microwave pulse is then applied which rotates the magnetization 90° such that it lies along the positive Y' axis (Figure 10b). If the frequency of the rotating frame equals the Larmor frequency of

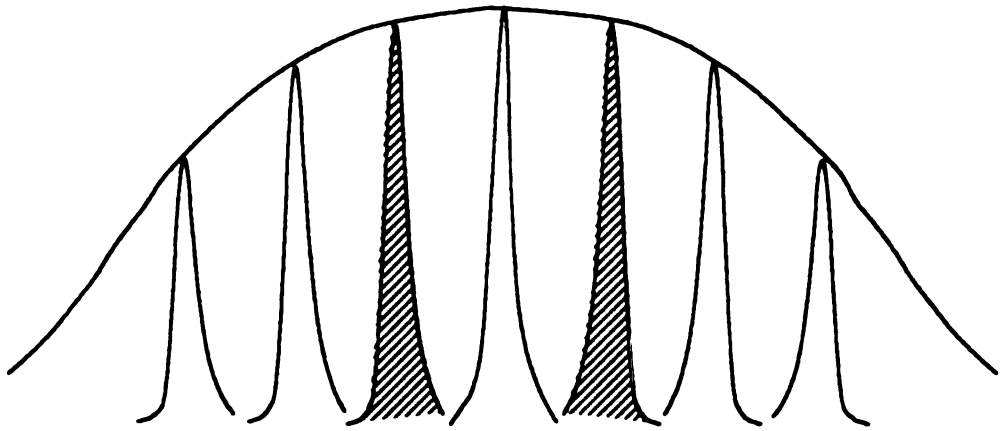

Figure 9: An inhomogeneously broadened line composed of individual spin packets.

Figure 10: A 2 pulse ESEEM experiment. Inset: Frequencies corresponding to two spin packets with respect to the frequency of the rotating frame. A) Net magnetization along the Z axis. B) Magnetization vector after the first pulse. C) Precession of individual spin packets after time τ. D) Location of the magnetization vector components after the second pulse. E) The formation of the spin echo.

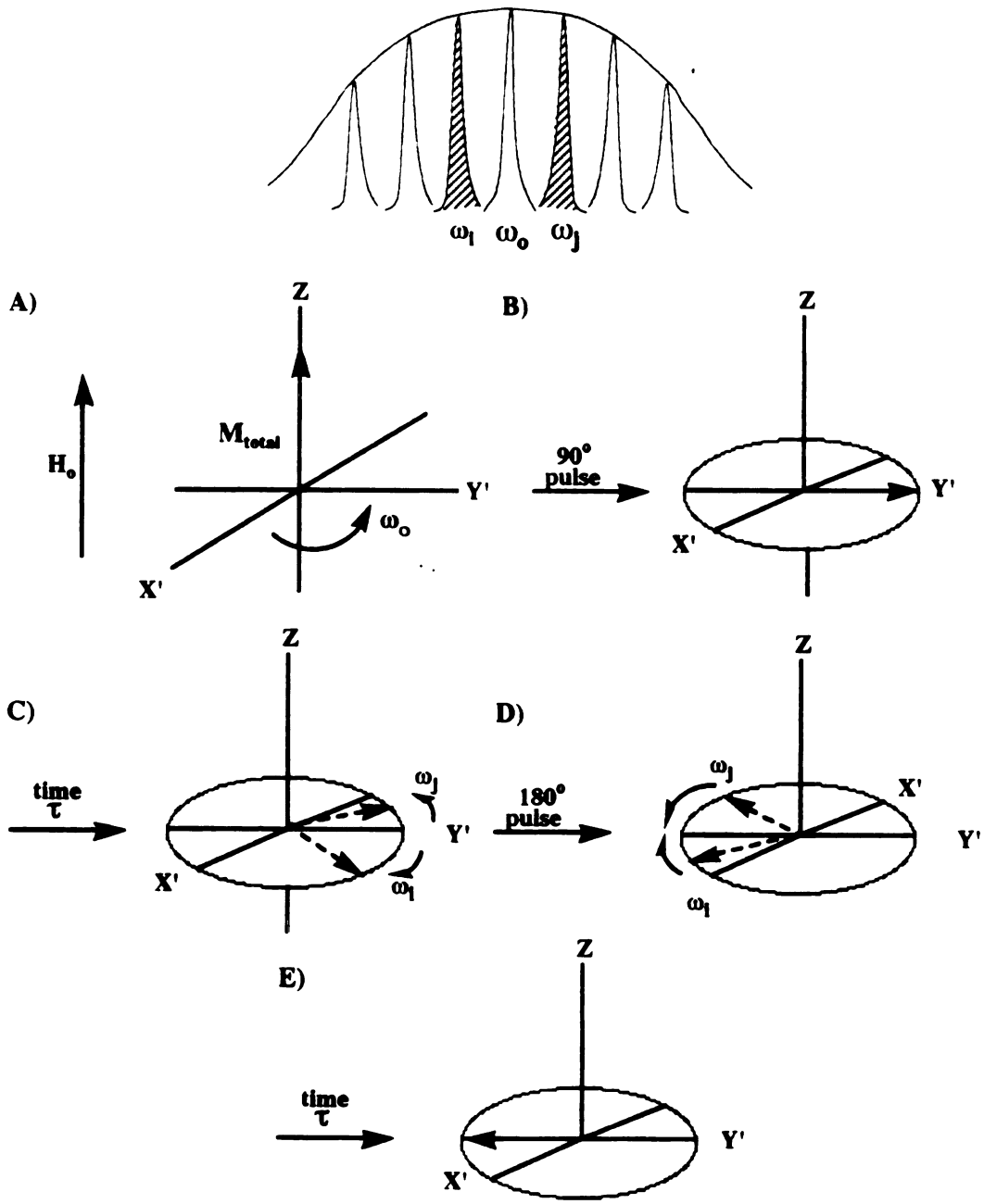

Figure 10

the magnetization, this vector will remain along the Y' axis. However, if the different spin packets have different offset frequencies, they will start to dephase. This dephasing is known as the free induction decay (FID), see Figure 10c. After a time τ, another microwave pulse is applied. This second pulse rotates the vectors 180° about the X' axis. The directions and the precessional frequencies of the individual components remain unchanged (Figure 10d). After time τ these components refocus along the -Y' axis (Figure 10e). The building up and decay of this -Y' magnetization is called a spin echo. The amplitude of this two pulse echo formation is a function of the pulse interval (τ) and the rate of decay of the echo (T_m, or the transverse relaxation time).

Nuclear modulation effect: Interactions that cause mixing of nuclear states such as anisotropic ligand hyperfine coupling lead to modulations of the spin echo amplitude as a function of τ. The nuclear modulation effect depends on a phenomenon called "branching of transitions," which in turn depends on all four transitions occurring.

Branching can be described accurately by the diagram in Figure 11. Consider an energy level diagram for the states S=1/2, I=1/2 (Figure 11, inset). Transitions A and C are allowed EPR transitions, B and D are previously forbidden transitions. The hyperfine frequencies are given by ω_{N1} and ω_{N2}. Again, the rotating frame (frequency= ω_0) will be used in this description. At a time τ after the 90° pulse, the spin packet corresponding to transition A (frequency= $\omega_A < \omega_0$) has dephased from the Y' axis of the rotating frame (Figure 11a). Again, a 180° pulse is applied. This time both transition A *and*, because of nuclear state mixing, transition C occur (Figure 11b). Transition C has its characteristic frequency, $\omega_C > \omega_0$. After time τ, the spin packet corresponding to transition A has rephased along the -Y' axis, however the spin packet corresponding to transition C has rotated past this point (Figure 11c). The echo amplitude is a measure of the projection of these vectors along the -Y' axis. The projection is a function of the angle between the two vectors (θ) and can be given by

Figure 11: Nuclear modulation effects. Inset: Energy levels corresponding to an S=1/2, I=1/2 system. Solid lines represent allowed transitions. Dashed lines represent semi-forbidden transitions. A) Location of the vector corresponding to transition A at time τ after the 90° pulse. B) Branching of transitions after the 180° pulse. C) The echo amplitude is given by the projection of the vectors on the Y' axis. This is a function of the angle θ between the two.

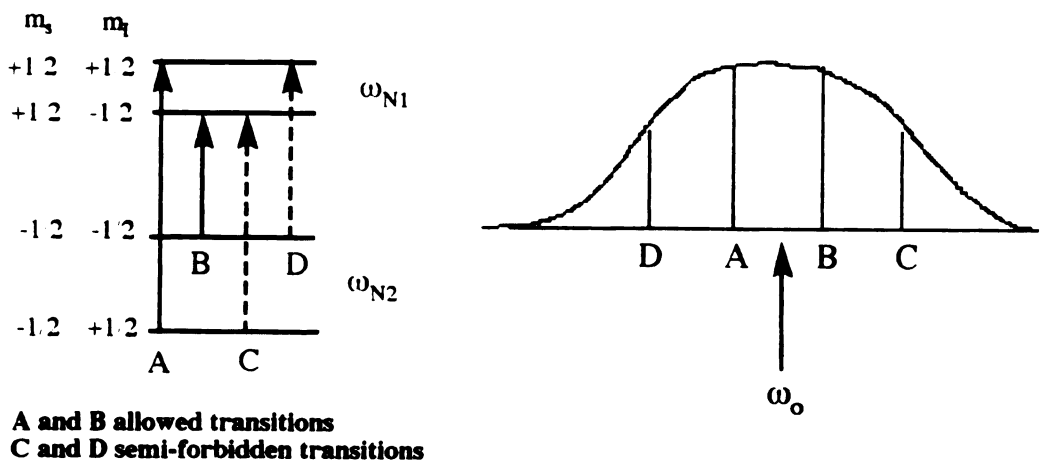

A and B allowed transitions
C and D semi-forbidden transitions

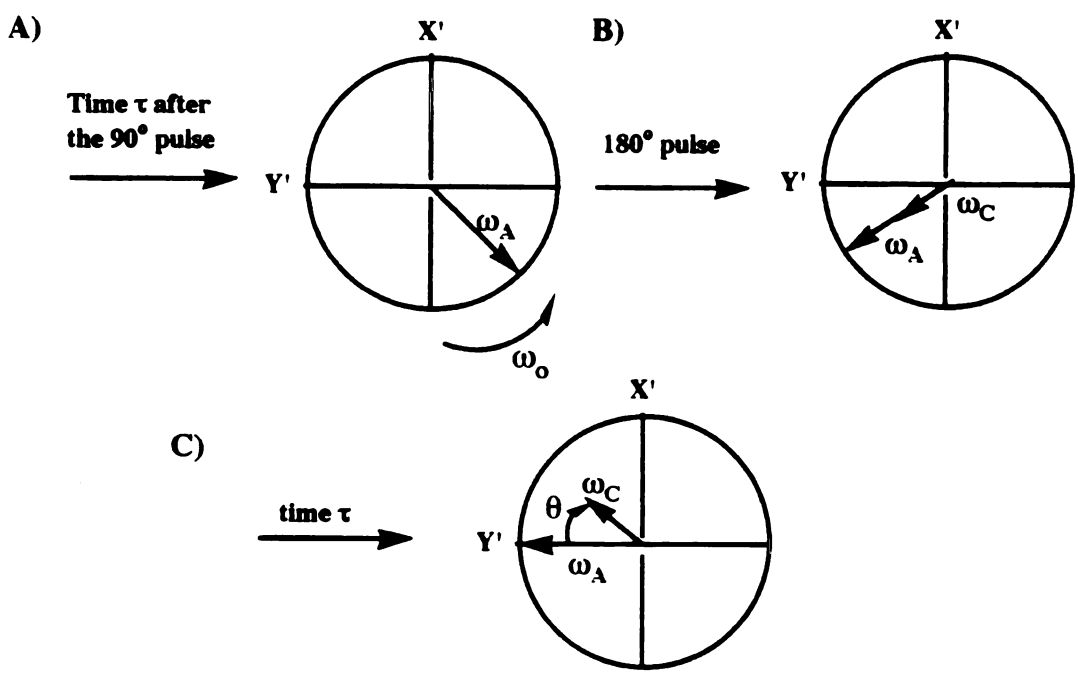

Figure 11

$$\theta = [\omega_A - \omega_C]\,\tau \qquad (15)$$

The difference between the two frequencies is given by the hyperfine frequence, ω_{N1}. The echo amplitude is then given by the expression

$$E(2\tau) = C_1 + C_2 \cos[\omega_{N1}(\tau)] \qquad (16)$$

where C_1 and C_2 represent transition probability amplitudes.

There are two conditions that preclude nuclear modulation effects, one quantum mechanical, the other instrumental. As previously mentioned, nuclear state mixing must occur in order for the branching to take place. The ability to excite all four transitions coherently is a combination of this quantum mechanical condition and an instrumental consideration: the microwave pulse must have sufficient energy to excite all four transitions. In ESEEM a 'hard' pulse, or a pulse containing a wide band of frequencies is used.

Chapter 3
Experimental

Materials and Methods: The development in 1981 of a PS II enriched thylakoid membrane preparation, free from other electron transfer proteins, yet still functional in terms of oxygen evolution, facilitated study of the PS II environment.[53] These so-called BBYs allowed direct spectroscopic studies and served as the starting point for the isolation of smaller membrane free complexes. This preparation relies on the fact that the thylakoid membranes, with their inherent negative charges, can be "stacked" by using divalent cations, such as Mg^{2+}. This increased lateral concentration can then be pelleted out by using selective solubilization methods. This treatment has been shown to remove 95% of the PS I from PS II. Only the light harvesting complex proteins and the PS II/OEC remain after completion of this procedure. Oxygen evolution studies performed on these BBY samples showed an increased oxygen evolution rate per chlorophyll. Additionally, it was found that the number of chlorophyll molecules per PS II had decreased from 400 chl/ PS II in thylakoids to 225-250 chl/PS II in BBYs. This decrease in the number of chlorophylls coupled with the loss of extraneous electron transfer proteins allowed direct examination of the PS II components, and particularly the Mn ensemble.

Previously, spectroscopic studies of the Mn complex were performed by using BBYs. The studies presented here, however, use a procedure that yields PS II components *without* the light harvesting complex. These preparations, first characterized by Ghanotakis et al in 1987, are called RCCs, and contain only the PS II components.[45]

PS II membrane samples from market spinach were isolated by using the method of Berthold et al[53] and diluted to a chlorophyll concentration of 2.5 mg chl/ml by using buffer A (see Figure 12 for a list of buffers used in the RCC procedure). These resuspended membranes were mixed with an equal volume of buffer B and incubated 10 minutes at 4° C in the dark. The non-ionic detergent n-octyl-β-D-glucopyranoside and

Buffer A(pH=6.0)
0.4 M sucrose
50 mM MES
10 mM NaCl

Buffer B(pH=6.0)
1.0 M sucrose
50 mM MES
0.8 M NaCl
10 mM $CaCl_2$
70 mM octyl glucaside

Buffer C (pH=6.0)
1.0 M sucrose
50 mM MES
0.4 M NaCl
5 mM $CaCl_2$

Buffer E(pH=6.0)
0.4 M sucrose
50 mM MES
10 mM NaCl
5 mM $CaCl_2$

Figure 12: Buffers used in the RCC procedure.

the high salt concentration were included in the buffer to solubilize PS II membranes and to facilitate the removal of the light harvesting complex proteins and the 17 and 23 kDa polypeptides. After the incubation, one part of the solubilized membranes was mixed with two parts of buffer C. This mixing was followed by centrifugation (90 minutes at 40,000 x g). The pellet, composed of the light harvesting complex and the solubilized membranes, was discarded. The supernatent, containing only PS II components was incubated on ice and an equal volume of 30% w/v polyethylene glycol (PEG) was added. This PEG precipitation step represents a modification to the original published procedure.[54] The PEG aggregates the water molecules causing "clumping" of the PSII constituents. These are then easily pelleted out using centrifugation. This solution was centrifuged 30 minutes at 40,000 x g. The resulting pellet was resuspended in buffer E and subsequently centrifuged 15 minutes at 40,000 x g. The final pellet was resuspended in buffer A containing 20 mM $CaCl_2$ (for the Ca^{2+} samples) or 20 mM $SrCl_2$ (for the Sr^{2+} samples). These samples were spun down into 4 mm O.D. EPR tubes, frozen while in the dark and kept at 77 K until EPR experiments could be performed.

The chelator samples were prepared by procedures similar to those used for the Ca^{2+} and Sr^{2+} samples. Again, market spinach was used to prepare PS II membranes in the manner of Berthold et al. The same protocol was used except for the PEG precipitation step. A contamination of the PEG resulted in the appearance of a spurious radical signal upon EPR analysis. To eliminate this signal the original dialysis step in the RCC procedure was followed. Further EPR studies indicated no difference between the dialyzed samples and the PEG precipitated samples (data not shown). Following the 90 minute centrifugation, the supernatant was dialyzed for one hour against a buffer containing 50 mM MES (pH= 6.0) and 10 mM NaCl (Spectrapor No. 6 dialysis tubing with M_r=12,000-14,000 cutoff was used). This dialysis step removes excess NaCl and sucrose by using a concentration gradient that subsequently causes aggregation of the PS

II components. Centrifugation for 20 minutes at 40,000 x g followed the dialysis step. The resulting pellet was resuspended to a concentration of 0.25 mg chl/ml by using buffer A. An equal volume of solution containing 2 M NaCl/buffer A (pH=6.0) was added to the RCC sample and this solution was incubated 30 minutes at 0° C in room light. The high salt concentration facilitates removal of the 17 and 23 kDa polypeptides. Incubation in the light permits S-state turnover and subsequent release of calcium. The chelator ethylene glycol β-bis-(amino ethyl) ether tetraacetic acid (EGTA) was added to a final concentration of 50 μM and the sample was centrifuged 20 minutes at 40,000 x g. Buffer A containing 50 μM EGTA was used to resuspend the pellet. Again, the sample was centrifuged (20 minutes at 40,000 x g). The supernatant was discarded and the pellet was resuspended in the dark by using a minimal amount of buffer A that contained 10 mM EGTA. The RCC sample was spun down into 4 mm OD EPR tubes and dark adapted for 30 minutes to ensure that all centers were in S_1. The samples were frozen in the dark and kept at 77 K until EPR studies could be performed.

Throughout both procedures, unless otherwise indicated, precautions were taken to maintain the temperature below 10° C and to use low light conditions so that maximal rates of oxygen evolution were retained.

EPR and ESEEM studies: Dark EPR spectra of the Sr^{2+} and Ca^{2+} samples at 8 K were recorded by using a Bruker ER200D spectrometer fitted with an Oxford Instruments ESR-900 cryostat. A Hewlett Packard 5245L electronic counter with a 5255A frequency converter plug in and a Bruker ER035M gaussmeter were used to measure microwave frequency and magnetic field, respectively. A rectangular TE_{102} cavity was used.

Dark adapted samples (5 minutes) were illuminated at 210 K in an ethanol/solid CO_2 mixture by using a 750 W projector. Illumination time was 8 minutes. Following illumination, the samples were frozen in the dark and the light spectra were recorded at 8 K. The spectra from both the dark and the illuminated Ca^{2+} sample correspond to an

addition of 30 accumulations. The spectra from the Sr^{2+} sample correspond to an addition of 60 accumulations. Signal averaging was accomplished by using an IBM PC fitted with a data analysis program written in house. The spectra presented in the following section, for both the Ca^{2+} and the Sr^{2+} samples, represent the difference between the illuminated spectrum and the dark adapted spectrum. Subtraction was carried out by using an IBM clone equipped with a subtraction program written in house. Spectrometer conditions accompany each figure.

Only the light spectrum of the chelator sample was recorded. The sample was dark adapted for 5 minutes and then illuminated according to the protocol above. This spectrum represents the addition of 30 accumulations. Spectrometer conditions accompany each figure.

ESEEM spectra of the illuminated samples were recorded at 1.8 K by only using a home-built ESEEM spectrometer previously described.[55] Data were collected by using only the two pulse (90-τ-180) microwave pulse sequence. The collection of ESE envelopes was controlled by an Apple McIntosh II computer. The Fourier transform of the ESE envelope was carried out with a modified version of the dead time reconstruction procedure that was developed by Mims.[56] For two pulse experiments the τ was varied from approximately 190 ns to 4 μs for each data set containing 1024 points. Other experimental conditions accompany each figure.

Chapter 4

Results and Discussion

RCC Characterization: The activity of enzymatic proteins present in biochemical pathways is often dependent on their location. Catalytic activity in a membrane bound complex may be decreased or lost upon its release from that membrane. This loss of activity may be concomitant with structural and, or, electronic rearrangements. Therefore, the presence or absence of a membrane bound complex can have direct effects on the function of that enzyme. This is seen in the transition from BBYs to RCCs. BBYs are composed of the membrane bound components and light harvesting proteins of PS II. In preparing RCCs from BBY membranes, the integrity of the membrane as well as the LHC is lost upon treatment of the samples with buffer containing the detergent, octyl-glucoside and a high concentration of NaCl. The elimination of these components directly affects subsequent biochemical manipulations. First, the calcium depletion procedure for BBYs requires extensive incubation of the membranes in the light. This incubation has to occur in the presence of chelators and in a high (2 M) salt buffer. This was found to be unnecessary for the RCC samples. The solubilization of the LHC and the removal of the 17 and 23 kDa polypeptides during the detergent washing facilitated spontaneous calcium release. Exclusion of calcium from subsequent buffers ensures maximum release of the cation. Reconstitution is easily accomplished with addition of either 20 mM $CaCl_2$ or, for strontium substituted samples, 20 mM $SrCl_2$.

Additionally, the dark adaptation needed for BBY samples is unnecessary for the RCCs. The BBY procedure includes a step whereby the membranes are incubated for 30 minutes at 0° C prior to storage.[44] RCC samples were centrifuged directly into the EPR tubes at 0° C in the dark without an additional dark adaption period. The centrifugation resulted in a highly concentrated sample, which proved to be ideal for spectroscopic

analysis. The EPR spectra of the RCCs not subjected to the dark prior to storage appeared similar to those obtained from BBYs. These spectra will be discussed further in an upcoming section.

As a direct consequence of the increased concentration of PS II that results from disruption of the membrane in BBYs and elimination of the light harvesting chlorophyll protein complexes, the absorption cross section of the RCC samples decreased. This effect was manifested practically as RCC samples were found to need additional illumination time (8 minutes instead of 5 minutes) to obtain maximum signal intensity.[44]

The use of the RCC preparation provided the increased concentrations of PS II needed for spectroscopic analysis. However, as a result of these increases, redefinition of the biochemical preparation procedure was needed.

The Mn complex and other components of the PS II/OEC had previously been studied by using samples that had been isolated according to the BBY procedure. These samples, containing both PS II components and the LHC, present some spectroscopic difficulties. The intensity of the multiline signal depends directly on the concentration of PS II, and specifically, the number of spins present in the sample. It is difficult to prepare BBYs at a concentration sufficient to generate the multiline spectrum without extensive signal averaging. The development and refinement of the RCC procedure has alleviated the concentration problems previously encountered, although PS II concentration is still low as an absolute basis in RCCs. Because these samples contain only PS II constituents, higher concentrations are attainable and, theoretically, this would indicate an increase in multiline signal intensity. However, complete spectroscopic characterization of the multiline signal from RCCs needs to be done before comparisons between the two procedures can be made. Additionally, the effect on the multiline of signal in RCCs of chelators, calcium depletion and reconstitution, or strontium substitution was not known. Spectroscopic studies of the multiline and modified multiline signals from RCC preparations are presented here. The similarities of these

spectra to those obtained from BBYs show that RCC preparations can be used in place of BBYs without the appearance of any spectroscopic anomalies.

EPR characterization: The difference spectrum from the S_2 state of the Ca^{2+} reconstituted RCC sample is presented in Figure 13a. This spectrum is the result of the difference between the spectrum recorded after illumination and the spectrum recorded after dark adaptation. This technique is used to subtract out signals which appear in both spectra and allows the multiline signal to be viewed in its entirety. The signal is centered at approximately g=2 and consists of 16-18 hyperfine lines split by an average of 92 gauss. The average hyperfine coupling was determined by direct measurement of the splittings between peaks off of the spectrum. This spectrum is similar to that obtained by Boussac and Rutherford for BBY samples which showed 16 lines and hyperfine couplings of 90 gauss.[44,46] Figure 13b shows the difference spectrum for the Sr^{2+} substituted samples. The signal is centered at approximately g=2 and consists of 16-18 hyperfine lines split by 71 gauss. Reconstitution with Sr^{2+} instead of Ca^{2+} results in losses, shifts, splittings and redistributions of the amplitude of the different lines. These modifications are similar to those seen by Boussac and Rutherford in Sr^{2+} reconstituted BBYs.[44,46] The hyperfine splitting in this case was found to be approximately 71 gauss. The overall shape of the signal, however, as well as its breadth was comparable to that seen in BBYs. These similarities indicate that the RCC samples can be substituted for the BBY samples in spectroscopic studies.

NaCl (1.2 M)/EGTA (50 μM) washing of PSII components results in the removal of Ca^{2+} and the inhibition of oxygen evolution.[65] This treatment precludes the appearance of the chelator modified multiline signal, which has only been detected by using high concentrations of chelator (10 mM) in the light. It is generated after illumination at 200 K and is attributed to a perturbation of the S_2 state. Characterization of this modified multiline signal was carried out by Boussac et al in BBY samples.[46]

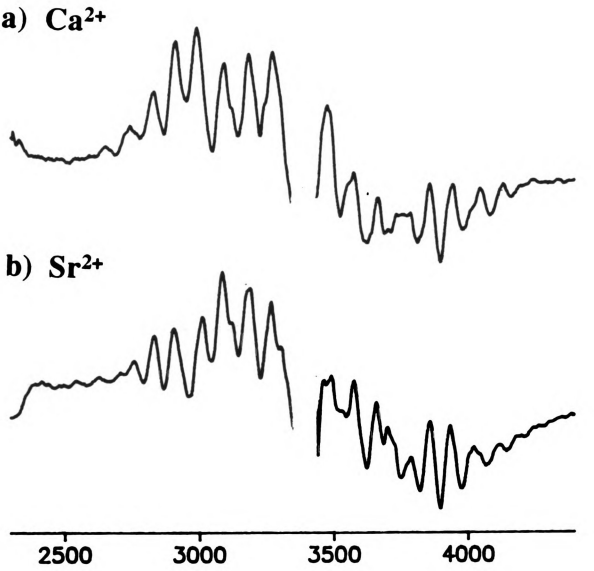

Figure 13: The light minus dark multiline spectrum of a) Ca^{2+} reconstituted RCCs and b) Sr^{2+} reconstituted RCCs. The spectra are the result of 30 (a) and 60 (b) signal averaged scans. Spectrometer conditions are as follows: scan range, 2000 G; center field, 3400 G; power, 10 dB; modulation amplitude, 20 Gpp; gain, 1.6×10^6; temperature, 8 K.

These researchers found a multiline signal with peak amplitudes approximately half of those found in the normal multiline signal. The modified multiline from RCC has not been characterized. Figure 14a shows the multiline signal from Ca^{2+} reconstituted RCC samples after 8 minutes of illumination at 200 K. The corresponding chelator modified multiline is presented in Figure 14b. The decrease in amplitude from the calcium to the chelator is obvious. Both spectra include the large feature at g=2 attributed to the Y_D^+ radical. This feature was subtracted out in previous spectra. The modifications are thought to arise from direct binding of the carboxylic acid substituent groups from the chelator to the Mn of the OEC. In the presence of calcium this interaction cannot occur, which has led to the suggestion that calcium plays a role in controlling ligand binding to Mn.[46]

Other spectroscopic features seen previously in BBY samples have been observed in EPR spectra from RCC preparations during the study described in this thesis. These include the EPR signal from g=2.0046 Y_D^+ (Signal II), from the iron quinone(g=1.9) and from cytochrome b559 (g_z=3.0, g_y= 2.1, data not shown).[57] These features correspond in amplitude and fine structure to those seen from BBY samples.

The EPR results from the RCC samples indicate that they are spectroscopically equivalent to the BBY samples. All spectral features in the Ca^{2+} reconstituted, Sr^{2+} substituted and chelator modified spectra are present. These RCC samples are free of spurious proteins and, therefore, are 2.5 times (75 μM as compared to 30μM in BBY) as concentrated as the BBYs.

Figure 14: Multiline spectra from a) Ca^{2+} reconstituted RCCs and b) EGTA treated RCCs. Spectrometer conditions are as in Figure 13. The spectra are the result of 25 (a) and 50 (b) signal averaged scans following illumination at 200 K.

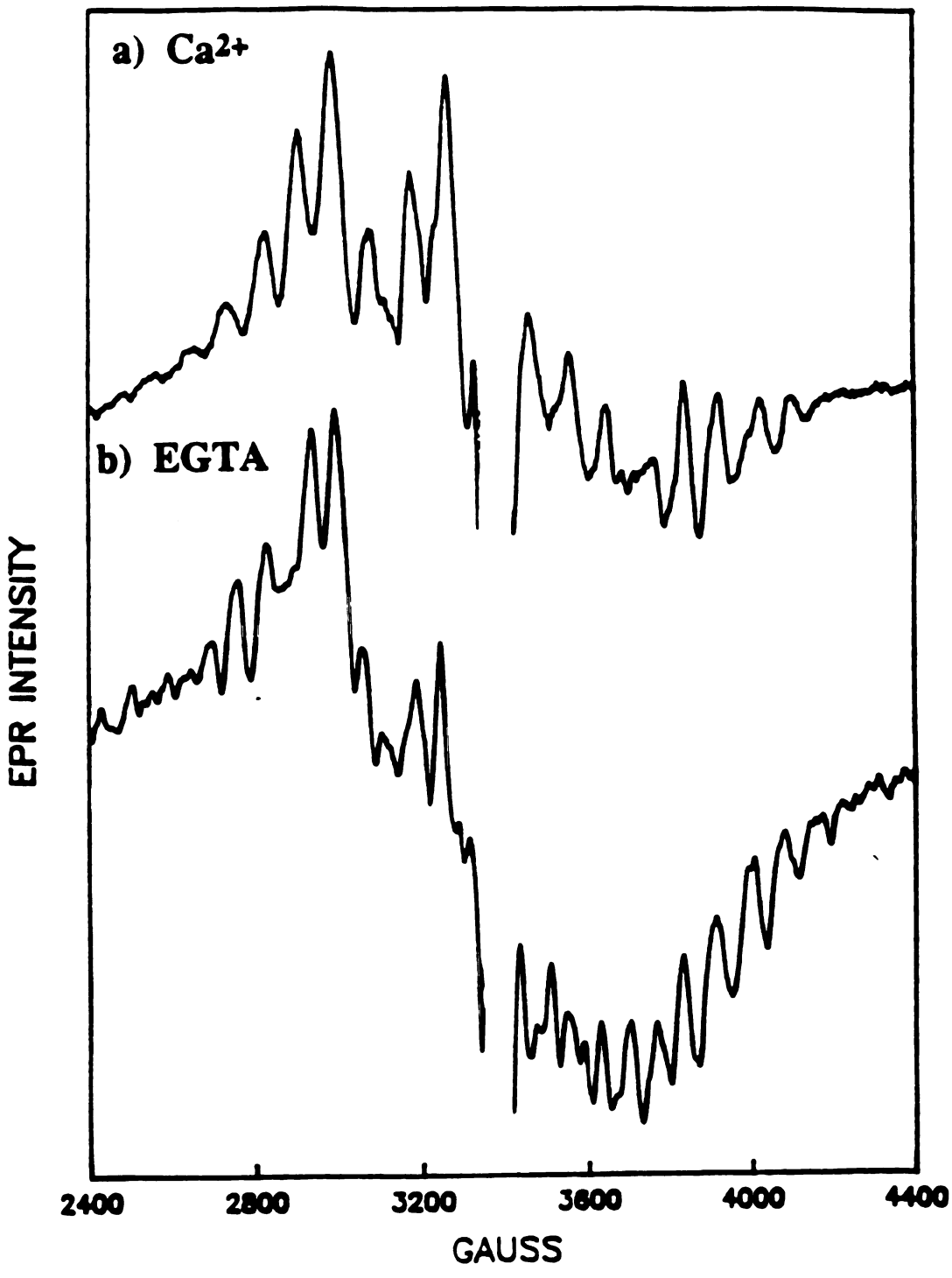
a) Ca2+
b) EGTA
EPR INTENSITY
2400
2800
3200
3600
4000
4400
GAUSS

ESEEM Studies of the Modified Multiline

Pulsed EPR studies of the multiline signal have focused on the signal from either spinach chloroplasts or cyanobacteria in the presence of calcium.[48-49] The effects of strontium substitution or chelator modification have not been explored. The modifications seen in the hyperfine structure of the continuous wave EPR experiments indicates a reorganization of spin densities and, or, exchange interactions in both the strontium and chelator samples. Changes in spin density may affect the interactions of the paramagnetic center with its environment. Both direct ligations and hydrogen bonds are affected by these changes. Britt and co-workers by using ESEEM techniques have recently identified a 4.5 MHz frequency that is attributed to a superhyperfine interaction of nitrogen with the Mn of the OEC.[49] This nitrogen has been proposed to be the nitrogen moeity of histidine.[49] The isotropic hyperfine coupling of a directly ligating nitrogen to the Mn of a dimanganese (III,IV) di-μ-oxo bridged bipyridine model compound was determined to be less than 1 gauss.[58] This coupling is too small to be seen with conventional continuous wave EPR. It is expected that the coupling of a nitrogen to the Mn ensemble of the OEC would resemble the coupling in the dimanganese compound. Researchers have been unsuccessful in resolving the nitrogen hyperfine and quadrupole parameters associated with this observed frequency. Analysis of these parameters can lead to identification and characterization of the interacting species. Additional double resonance and multi-frequency experiments will need to be performed to identify these parameters (see Future Work section, Chapter 5).

Both strontium and EGTA treatments result in a modification of the continuous wave multiline spectrum, as described above. Interactions between the paramagnet and the strontium or the carboxylate groups of the chelator seem to be the source of these changes. Small structural changes can also affect the hyperfine interaction through the Fermi contact term of the hamiltonian and the magnitude of the exchange interaction. In

this study, the effect of strontium and chelator on the proposed nitrogen coupling will be addressed by using ESEEM on RCC samples.

Figure 15a is the time domain and Figure 15b the Fourier transform of a 2 pulse ESEEM experiment performed on the Ca^{2+} reconstituted sample. Three features are apparent in the FT spectrum. Two of these, the peaks at 14.553 and 29.249 MHz, can be attributed to interactions with protons in the immediate environment of the paramagnet (ν_H= 14.48 at 3400 G). The third feature, a peak at 4.110 MHz is similar in intensity and frequency to peaks seen in both BBYs and cyanobacteria experiments performed by DeRose and co-workers and Britt and co-workers.[48-49]

The 4 MHz feature was initially observed in ESEEM experiments that established ammonia binding to the Mn of the OEC. The source of the signal at that time was unknown. It was observed in BBYs with and without ammonia present. It was postulated that the signal arose from a component within the OEC, possibly a manganese ligand. The identity of this ligand was not confirmed, although nitrogen was suggested. It was not until further ESEEM experiments were performed in 1990 by DeRose and co-workers that a source for the signal was determined.[49] In these experiments cyanobacteria were grown on a medium in which the only source of nitrogen was from added $K^{15}NO_3$. A control experiment was run whereby only $K^{14}NO_3$ was used. The 4 MHz peak was seen only in the control experiment. This led to the conclusion that it must arise from a nitrogen ligand to the Mn of the OEC.[49] This origin of this nitrogen is controversial. The proposed Mn binding regions on the D1 and D2 polypeptides have several nitrogen containing amino acid residues that are conserved among cyanobacteria and higher plants.[59] Of these amino acids (lysine, arginine and histidine) the only one that is known to coordinate to manganese containing proteins is histidine.[49] This suggests histidine as the source of the ligating nitrogen.

The substitution of strontium for calcium in the RCC samples led to a modified multiline signal. These modifications were observed in both the number of peaks and

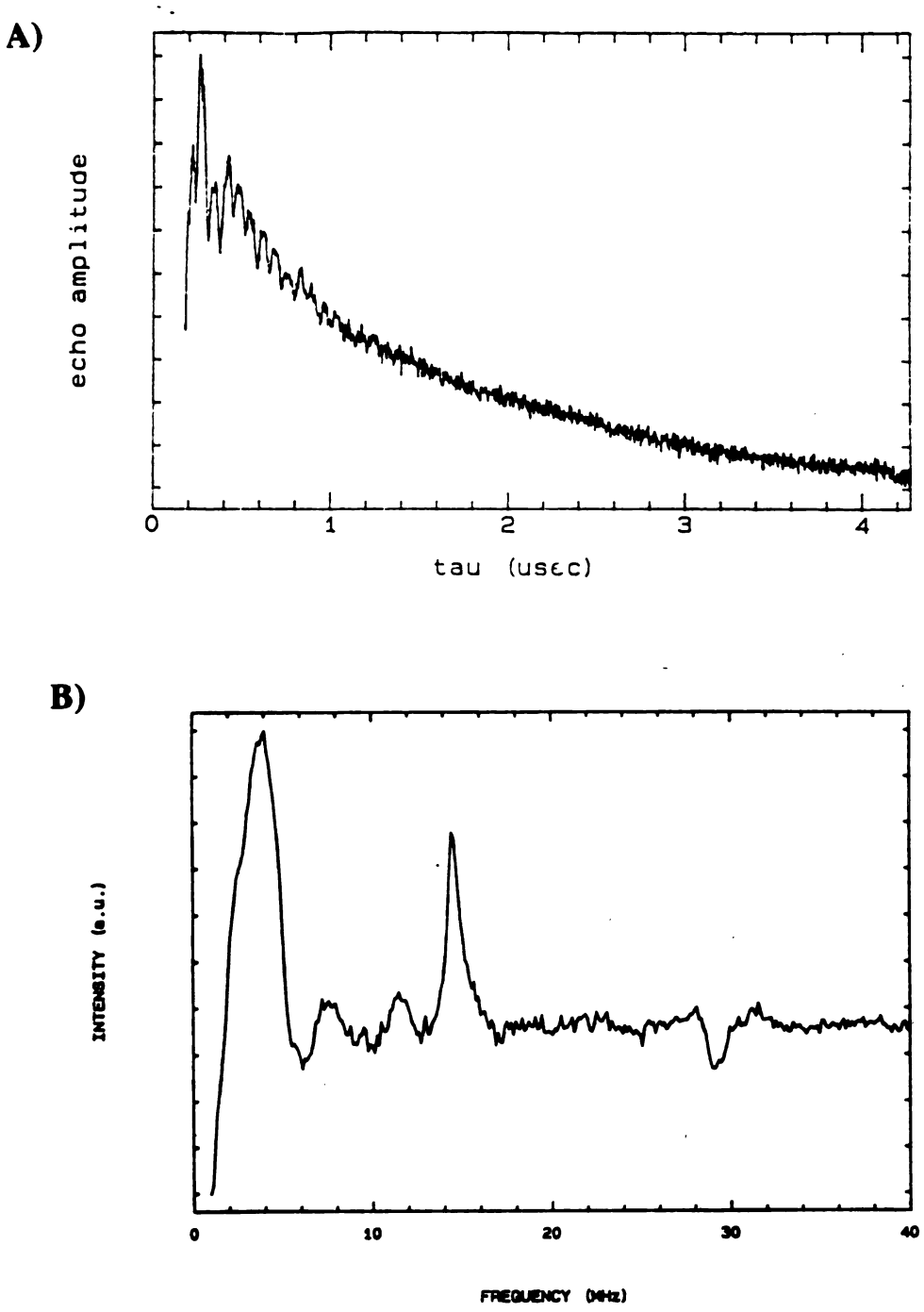

Figure 15: Two pulse ESEEM (a) and Fourier cosine transfer (b) for the Ca^{2+} reconstituted sample. Measurement conditions for the data shown are: microwave frequency, 8.893 GHz; magnetic field strength, 3400 G; pulse power, 25 W; pulse width, 15 ns FWHH; tau value, 140 ns; sample temperature, 1.8 K; repetition rate, 60 Hz.

their splittings and intensities. Modifications of this type are thought to arise from conformational changes that result in redistribution of electron spin density. If these structural changes are of sufficient magnitude they will perturb the interactions between the paramagnet and ligating magnetic nuclei. This perturbation should be apparent in the ESEEM spectrum. The 2 pulse time domain (Figure 16a) and Fourier transform (Figure 16b) spectra from the Sr^{2+} RCC samples are identical in appearance to the spectra from the Ca^{2+} samples. The peak at 4.106 MHz correponds to the peak attributed to nitrogen seen in the Ca^{2+} samples. The ESEEM spectra from the EGTA treated samples are presented in Figure 17. The Fourier transform (Figure 17b) of the time domain data exhibits a peak in the 4 MHz range. These data are very similar to those seen for the calcium and strontium samples. This indicates that the electronic interaction of the nitrogen with the Mn has been unaffected by the substitutions. There are several possible explanations for this. First, the substitution of strontium or EGTA could affect only the electronic interactions within the Mn cluster without affecting the interaction of the ligand. This structural rearrangement causes changes in the Mn hyperfine interactions that are apparent in the continuous wave EPR spectrum but do not affect the nitrogen couplings seen in the ESEEM spectrum. A second possible explanation is that substitution of strontium induces a conformational change that does not affect the site of nitrogen ligation. Therefore the interactions of the nitrogen and the manganese are not affected. A final explanation for these similarities is that there is a structural change upon strontium or chelator substutition that results in the modified multiline signal, however there is a simultaneous change in either the bond angle or orientation of the nitrogen that offsets this conformational change. The exact explanation for this phenomenon requires additional spectroscopic techniques that will be discussed in the following section.

The use of a refined biochemical preparation which increases the concentration of PS II present in a sample has facilitated study of the Mn multiline EPR spectrum

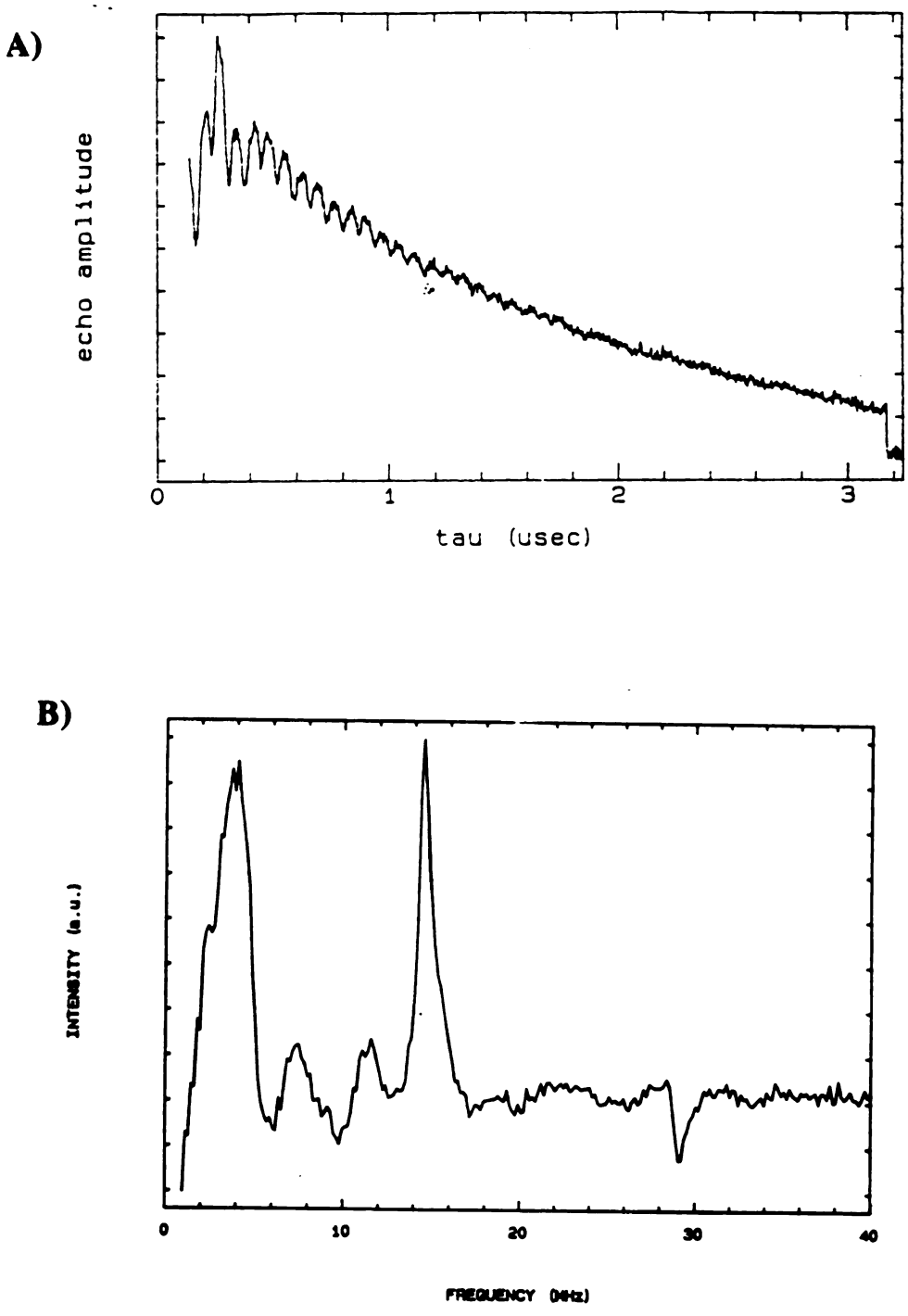

Figure 16: Two pulse ESEEM (a) and Fourier cosine transfer (b) for the Sr^{2+} reconstituted samples. Spectrometer conditions were as in Figure 15.

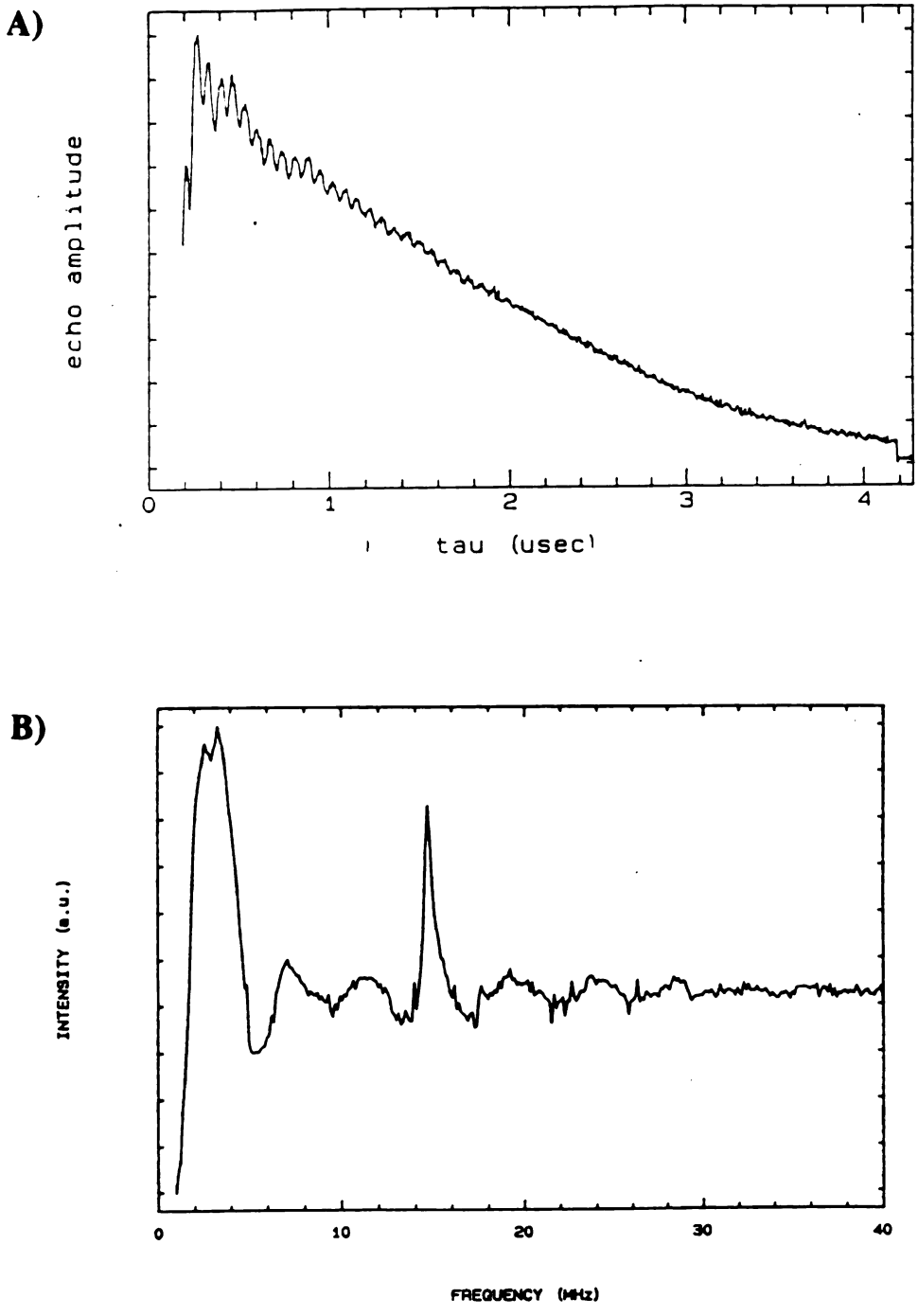

Figure 17: Two pulse ESEEM (a) and Fourier cosine transfer (b) for the EGTA treated sample. Spectrometer conditions were as in Figure 15.

associated with the S_2 state of the OEC. This spectrum, which is thought to arise from exchange coupling of two, three or four mixed valence Mn atoms, has been studied by using magnetic resonance techniques. EPR studies discussed in this thesis have shown that the RCC samples are spectroscopically equivalent to their predessors. The increased concentration achieved with the RCCs is essential for EPR analysis. Slight modifications of the published RCC procedure were made as a result of this increased concentration. It has been shown previously that substitution of Sr^{2+} or chelator into calcium depleted BBY samples causes modifications in the hyperfine splitting seen in the multiline spectrum. These differences are thought to arise from perturbations of the Mn exchange coupling. These differences were present in the multiline spectra from the RCC samples presented in this thesis. ESEEM studies of the RCC samples were also performed. A 4 MHz peak, thought to arise from coupling to a ligated nitrogen, is present in all spectra recorded. This indicates a conformational change that does not affect the interactions of the Mn with its environment. Additional magnetic resonance studies will be performed to determine the magnitude of these interactions.

Chapter 5
Future Work

Quantitative analysis of the proposed nitrogen ligations to the Mn cluster of the OEC has not been possible by using continuous wave and spin echo EPR techniques. Neither the hyperfine coupling parameters nor the nuclear quadrupole parameters have been determined for this interaction. These parameters can be used to characterize the interacting species more completely. From this information, additional knowledge can be gained about the structure of the OEC. To resolve the peaks corresponding to these types of transitions other techniques must be employed. Pursuit of these techniques is the topic of this chapter.

ESE detected ENDOR: The development of pulsed-EPR schemes that use electron spin echoes to determine ENDOR frequencies by Mims[60] and Davies[61] has allowed further study of systems in which small hyperfine interactions are poorly resolved using conventional ESEEM techniques. The theory of ESE detected ENDOR is based upon the double resonance technique developed for pulsed NMR spectroscopy. The pulse sequence for the Davies ESE-ENDOR is given in Figure 18. In this experiment a 180^{o} pulse of microwave radiation is applied to the electron spins followed by a radio frequency pulse of duration T. This is followed by the conventional Hahn pulse sequence (90^{o}-τ-180^{o}). The spin echo appears at time τ after the final 180^{o} pulse. The effect on the spectrum can be understood with the aid of Figure 18 for an S=1/2, I=1/2 system. At thermal equilibrium the population of the lower spin states is slightly higher than the population of the upper states (this is shown with the relative lengths of the bars in Figure 18). Assuming a microwave pulse frequency that is resonant with only one EPR transition, the initial 180^{o} pulse inverts the populations of the levels corresponding to that EPR transition. If the rf pulse is resonant, with either NMR transition, then the population difference between these two levels will be equalized and the electron spin

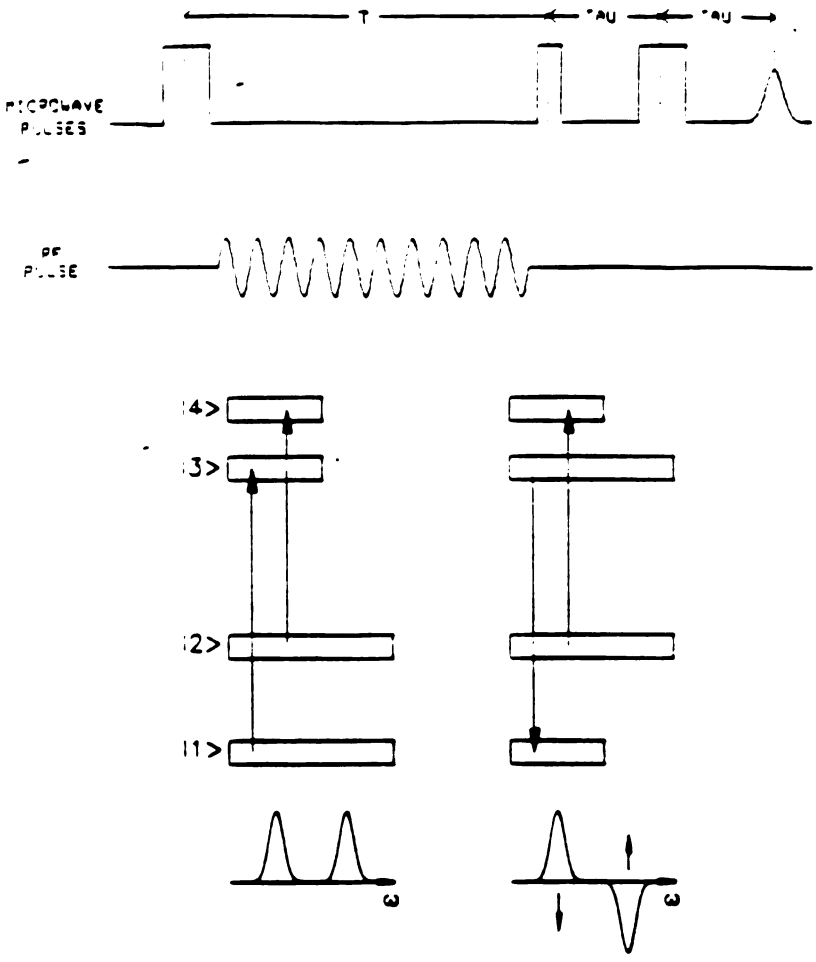

Figure 18: Davies ESE-ENDOR pulse sequence (top). Energy level diagram for a coupled S=1/2, I=1/2 system. The diagram on the left shows the level populations at thermal equilibrium while that on the right shows the level populations after a selective 180° pulse resonant with the 1-3 transition has been applied.

echo amplititude will disappear. An ENDOR spectrum can be generated by plotting the ESE amplitude as a function of rf pulse frequency.[62] Recent studies have shown that the ^{14}N couplings in the protein Stellacyanin can be resolved in the 1-60 MHz region. The ESE-ENDOR spectrum from this protein compares well with the continuous wave ENDOR spectrum.[63] The advantage in using the ESE-ENDOR method over conventional ENDOR rests in the data acquisition time period. The ESE-ENDOR spectrum was collected in 12 minutes while the ENDOR spectrum took 1.5 hours to acquire. The application of this technique to the PS II/OEC system should provide a more sensitive and systematic means by which to measure hyperfine interactions. There are additional advantages to using this method. It provides both increased sensitivity and a systematic means of collecting data.

Characterization of the S_3 EPR signal: Boussac et al[64] reported an EPR signal attributed to the S_3 state of the OEC. This signal, found in calcium depleted BBYs, is centered around g=2 and has a width of approximately 164 gauss. It is generated by illumination of the samples at 273 K, followed by freezing while the sample is still under illumination. It was later shown that EDTA, EGTA or citrate were required in order to observe this signal. The source of this signal is still controversial. It has been suggested that this signal results from the interaction of the manganese ensemble with a nearby oxidized histidine residue.[65] It is unknown whether this oxidation occurs as a part of the normal S state transitions or whether it is a direct consequence of the calcium depletion. Recently, however, Hallahan et al[66] proposed that the S_3 state signal arose from Y_Z, a tyrosine radical. This was based on the observation that, at 50 K, the signal associated with the tyrosine radical increased relative to that of the S_3 signal. This was immediately challenged by Boussac and Rutherford[67] who cite power saturation artifacts as the source of this $Y_Z^{\cdot}$ signal increase. The assignment of the split S_3 signal to a histidine radical remains unproven and controversial.

The S_3 signal has recently been generated in this laboratory, however complete spectroscopic analysis of the signal has not been performed. ESEEM experiments can provide information about the small hyperfine couplings that may be masked by the broad featureless signal. The signal, which has been determined to be centered at g=2 with a linewidth of 148 gauss, appears to be inhomogeneously broadened. Spectroscopic studies in which both ENDOR and ESEEM are used will be undertaken to further resolve this signal.

PS II Mutants: In conjuction with Professor Lee McIntosh's lab in the Plant Research Laboratory the characterization of cyanobacteria lacking PS I will be performed . Site directed mutagenesis techniques have been employed to remove the gene necessary to assemble the PS I components of photosynthesis. By eliminating this reaction center, purification of the PS II system has been simplified resulting in preparations that have increased oxygen evolving activity. Preliminary EPR data shows a multiline spectrum similar to that obtained from BBYs. ESEEM experiments have been performed on this PS I minus mutant and the 4 MHz peak associated with nitrogen has been observed. An additional lower frequency peak has also been seen, although no assignment has been made thus far.

Further mutations of this PS I minus sample are planned. The D1 polypeptide has been identified as a potential site of Mn ligation by several groups.[12] Mutations in this polypeptide, and in particular of Asp-170, have resulted in loss of photoautotrophic growth. This loss occurred when Asp-170 was replace with 14 out of 16 residues or when Asp-242 was replaced with Gln, Ala or Val.[68] Evidence that these or other amino acid residues ligate either the Mn ensemble or the calcium co-factor must come from spectroscopic analysis. Spectroscopic data, however, has only been reported for mutations constructed at Asp-170 of the D1 polypeptide. Complete spectroscopic characterization of the mutants obtained from Professor McIntosh's lab is planned.

Bibliography

Bibliography

1 Hill, R. and Bendall F. (1960) *Nature 186,* 136.

2 Staehelin L.A. (1986) in *Encyclopedia of Plant Physiology, New Serices, Volume 19, Photosynthesis III,*(L.A. Staehlin and C.J. Arntzen,eds.) Springer-Verlag, Berlin, 476.

3 Babcock, G.T., Barry, B.A., Debus, R.J., Hoganson, C.W., Atamian, M., McIntosh,L., Sithole, I., and Yocum, C.Y. (1989) *Biochemistry, 28,* 9557.

4 Ghanotakis, D.F., Topper, J.N. and Yocum, C.F. (1984) *Biochim Biophys Acta, 767,* 524.

5 Enami, I., Kaneko, M., Kitamua, N., Koike, H., Sonoike, K., Inoue, Y., and Katoh, S. (1991) *Biochim Biophys Acta, 1060,* 224.

6 Hoganson, C.W., Babcock, G.T., and Yocum, C.F. (1989) *Photosynth. Res., 22,* 285.

7 Nakatani, H.Y. (1984) *Biochim. Biophy. Res. Commun., 120,* 299.

8 Nanba, O. and Satoh, K. (1987) *Proc. Natl. Acad. Sci. U.S.A., 84,* 109.

9 Diesenhofer, J., Epp, O., Miki, K., Huber, R., and Michel, H. (1985) *Nature, 318,* 618.

10 Sayre, R.T., Andersson, B., and Bogorad, L. (1986) *Cell, 47,* 601.

11 Debus, R.J., Barry, B.A., Sithole, I., and Babcock, G.T. (1988) *Biochemistry, 27,* 9071.

12 Rutherford, A.W. (1989) *Trends. Biochem. Sci., 14 (6),* 227.

13 Ghanotakis, D.F., Demetriou, D.M., and Yocum, C.F. (1987) *Biochim.Biophys. Acta, 891,* 15.

14 Bowlby, N.R., Ghanotakis, D.F., Yocum, C.F., Petersen, J., and Babcock, G.T., (1988) *Light Energy Transduction in Photosyntheisi: Higher Plant and Bacterial Models* (Stevens, S.E. Jr., and Bryant, D.A., Eds.) p. 215, The American Society of Plant Physiology Publishers, Baltimore, MD.

15 Babcock, G.T., Widger, W.R., Cramer, W.A., Oertling, W.A., and Metz, J.G. (1985) *Biochemistry, 24,* 3638.

16 Nuijs, A.M., Van Gorkom, H.J., Flijter, J.J., and Duysens L.N.M. (1986) *Biochim. Biophys. Acta, 848,* 167.

17 Crofts, A.R. and Wraight, C.A. (1983) *Biochim. Biophys. Acta,726,*149.

18 Witt, H.T.,Schlodder, E., Brettel, K., and Saygin, O. (1986) *Photosynth. Res., 10,* 453.

19 Barry, B.A. and Babcock, G.T. (1987) *Proc. Natl. Acad. Sci. U.S.A., 84,* 7099.

20 Debus, R.J., Barry, B.A., Babcock, G.T., and McIntosh, L. (1988) *Proc. Natl. Acad. Sci. U.S.A., 85,* 427.

21 Barry, B.A. and Babcock, G.T. (1988) *Chem Scr 28A,* 117.

22 Klimov, V.V., Allakhverdiev, S.I., Demeter, S., Krasnovskii, A.A. (1980) *Dokl. Akad. Nauk. SSSR, 249,* 227.

23 Joliot, P., Barbieri, G., and Chabaud, R. (1969) *Photochem. Photobiol., 10,* 309.

24 Kok, B., Forbush, B., and McGloin, M. (1970) *Photochem. Photobiol., 11,*457.

25 Babcock, G.T. (1973) PhD thesis, Department of Chemistry, University of California, Berkeley, Lawrence Berkeley Laboratory Report LBL-2172.

26 Babcock, G.T. (1987) *The Photosynthetic Oxygen Evolving Process. In: New Comprehensive Biochemistry* (Ed.: Amesz, J.) Elsevier, Amsterdam, 125.

27 Pirson, A. (1937) *Z. Bot. 31,* 193.

28 Cheniae, G.M. and Martin, I.F. (1966) *Brookhaven Symp. Biol. 19,* 406.

29 Yocum, C.F., Yerkes, C.T., Blankenship, R.E., Sharp, R.R., and Babcock, G.T. (1981) *Proc. Natl. Acad. Sci. U.S.A., 78,* 7507.

30 Kirby, J.A., Robertson, A.S., Smith, J.P., Thompson, A.C., Cooper, S.R.,and Klein, M., (1981) *J. Am. Chem. Soc., 103,* 5529.

31 Yachandra, V.K., Guiles, R.D., McDermott, A.E., Britt, R.D., Dexheimer, S.L., Sauer, K., and Klein M. (1986) *Biochim. Biophys. Acta, 850,* 324.

32 Penner-Hahn, J. (1990) *J. Am. Chem. Soc.,112,* 2549.

33 Dismukes, G.C. and Siderer, Y. (1980) *FEBS Lett., 121,* 78.

34 Dismukes, G.C. and Siderer, Y. (1980) *Proc. Natl. Acad. Sci. U.S.A.,78,* 274.

35 Brudvig, G.W., Casey, J.L., and Sauer, K. (1983) *Biochim. Biophys. Acta, 723,* 366.

36 Forbush, B., Kok, B., and McGloin, M. (1971) *Photochem. Photobiol., 11,* 457.

37 Inoue, Y. and Shibata, K. (1978) *FEBS Lett., 85,* 193.

38 Larson, E., Haddy, A., Kirk, M.L., Sands, R.H., Hatfield, W.E., and Pecoraro, V. (1991) *J. Am. Chem. Soc.,112,* 2549.

39 Bhula, R., Gainsford, G.J., and Weatherburn, D.C. (1988) *J. Am. Chem. Soc., 110,* 7550.

40 Dismukes, G.C., Ferris, K., and Watnick, P. (1982) *Photochem. Photobiol.,3,*243.

41 Bonvoisin, J., Blondin, G., Girerd, J.J., and Zimmerman, J.L.(1992) *Biophys. J., 61,* 1076.

42 England, R.R. and Evans, E.H. (1981) *FEBS Lett., 143,* 175.

43 Ghanotakis, D.F., Babcock, G.T., and Yocum, C.F. (1984) *FEBS Lett., 167,* 127.

44 Boussac, A. and Rutherford, A.W. (1990) *FEBS Lett., 277,* 69.

45 Ghanotakis, D.F., Babcock, G.T., and Yocum, C.F. (1984) .*Biochim. Biophys. Acta,,765,* 388.

46 Boussac, A., Zimmerman, J.L. and Rutherford, A.W.(1990) *FEBS Lett., 277,* 69.

47 Andreasson, L.E. (9189) *Biochim. Biophys. Acta ,973,* 465.

48 Britt, R.D., Simmerman, J.L., Sauer,K., and Klein, M. (1989)*J. Am. Chem. Soc., 111,*3522.

49 DeRose, V.J., Yachandra, V.K., McDermott, A.E., Britt, R.D., Sauer, K., and Klein, M. (1990) *Biochemistry, 30,* 1335.

50 Wertz, J.E. and Bolton, J.R. (1986) *Electron Spin Resonance: Elementary Theory and Applications,* Chapman and Hall, New York.

51 Palmer, G. (1980) *Electron Paramagnetic Resonance in: Methods for Determining Metal Ion Environments in Proteins* (Eds.: Darnell, D.W. and Wilkins, R.G.) Elsevier, North-Holland, 153.

52 Schweiger, A. (1991) *Angew. Chem, int. Ed. Engl., 30,* 265.

53 Berthold, D., Babcock, G.T. and Yocum, C.F. (1981) *FEBS Lett., 134,* 231.

54 Bowlby, N.R.(1989) PhD thesis,Department of Chemistry, University of Michigan , Ann Arbor, MI

55 McCracken, J.L.

56 Mims, W.B. (1984) *J. Magn. Res., 59,* 291.

57 Miller, A. F. and Brudvig, G.W. (1991)*Biochim. Biophys. Acta, 1056,* 1.

58 Britt, R.D. (1988) PhD thesis, Department of Physics,University of California Berkeley, Lawrence Berkeley Laboratory.

59 Gingrich, J.C., Gasparich, G.E., Sauer, K. and Bryant, D.A. (1990) *Photosyn. Res.,24,* 137.

60 Mims, W.B. (1965)*Proc. Roy. Soc. A, 283,* 452.

61 Davies, E.R. (1974) *Phys. Lett., 47A,* 1.

62 Mehring, M., Hofer, P., Grupp, A. (1986) *Phys. Rev. A,33,* 3523.

63 Roberts, J.E., Brown, T.G., Hoffman, B. M., and Peisach, J. (1980) *J. Am. Chem. Soc., 102,* 825.

64 Boussac, A. and Rutherford, A.W. (1988) *Biochemistry, 27,* 3476.

65 Boussac, A., Zimmerman, J.L., Rutherford, A.W. and Lavergne, J. (1990), *J. Am. Chem. Soc,347,*303..

66 Hallahan, B.J., Nugent, J.H.A., Warden, J.T., and Evans, S.M.C.W. (1992) *Biochemistry, 31,* 4562.

67 Boussac, A. and Rutherford, A.W. (1992) *Biochemistry*, in press.

68 Diner, B.A., Nixon, P.J., and Farchans, J.W. (1991) *Current Opinion In Struct. Biol.,1,* 546.